AALBORG UNIVERSITY

DENMARK

A Novel Distributed Secondary Coordination Control Approach for Islanded Microgrids

Lu, Xiaoqing; Yu, Xinghuo; Lai, Jingang; Wang, Yaonan; Guerrero, Josep M.

A Novel Distributed Secondary Coordination Control Approach for Islanded Microgrids

Xiaoqing Lu, Xinghuo Yu, *Fellow, IEEE*, Jingang Lai, Yaonan Wang, and Josep M. Guerrero, *Fellow, IEEE*

Abstract—This paper develops a new distributed secondary cooperative control scheme to coordinate distributed generators (DGs) in islanded microgrids (MGs). A finite time frequency regulation strategy containing a consensus-based distributed active power regulator is presented, which can not only guarantee the active power sharing but also enable all DGs' frequencies to converge to the reference value within a finite time. This enables the frequency and voltage control designs to be separated. Then an observer-based distributed voltage regulator involving certain reactive power sharing constraints is proposed, which allows different set points for different DGs and, thus, accounts for the line impedance effects. The steady-state performance analysis shows that the voltage regulator can accurately address the issue of global voltage regulation and accurate reactive power sharing. Moreover, all the distributed controllers are equipped with bounded control inputs to suppress the transient overshoot, and they are implemented through sparse communication networks. The effectiveness of the control in case of load variation, plug-and-play capability, communication topology change, link failure, time delays and data drop-out are verified by the simulation of an islanded MG in MATLAB/SimPowerSystems.

Index Terms—Distributed control, islanded microgrids, secondary control, finite time regulator

NOMENCLATURE

N	Number of DGs in an islanded MG.
ω_i^{nom}	Nominal set point for DG$_i$'s frequency.
v_i^{nom}	Nominal set point for DG$_i$'s voltage.

ω^{ref}	Frequency reference value.
v^{ref}	Voltage reference value.
$\omega_i(v_i)$	DG$_i$'s frequency (voltage magnitude).
$P_i(Q_i)$	DG$_i$'s active (reactive) power.
$P_{i,\mathrm{max}}$	Maximum capacity of DGi's active power.
$Q_{i,\mathrm{max}}$	Maximum capacity of DGi's reactive power.
$K_i^P(K_i^Q)$	Active (reactive) power droop coefficient.
$u_i^\omega(u_i^v)$	Frequency (voltage) control input for DG$_i$.
$u_i^p(u_i^q)$	Active (reactive) power control input for DG$_i$.
$\hat{v}_i$	Estimated value for voltage v_i.
$\mathcal{G}^\omega(\mathcal{G}^v)$	Cyber network for frequency (voltage).
$\mathcal{G}^p(\mathcal{G}^q)$	Cyber network for active (reactive) power.
$N_i^\omega(N_i^v)$	Neighbor sets for DG$_i$'s frequency (voltage).
$N_i^p(N_i^q)$	Neighbor sets for DG$_i$'s active (reactive) power.
$A^\omega(A^v)$	Adjacency matrix of $\mathcal{G}^\omega$ ($\mathcal{G}^v$) with elements $a_{ij}^\omega(a_{ij}^v)$.
$A^p(A^q)$	Adjacency matrix of $\mathcal{G}^p$ ($\mathcal{G}^q$) with elements $a_{ij}^p(a_{ij}^q)$.
$B^\omega(B^v)$	Leader adjacency matrix for frequency (voltage).
L^v	Laplacian matrix of A^v.
μ	Normalized positive left eigenvector corresponding to the zero eigenvalue of irreducible matrix L^v.
$\mathrm{sign}(\cdot)$	Sign function.
$\mathrm{sig}(\cdot)^\alpha$	$\mathrm{sign}(\cdot)|\cdot|^\alpha$ with the factional power $\alpha \in (0,1)$.
$\mathrm{sat}(\cdot)$	Saturation function.
$\mathrm{sat}_\delta(\cdot)$	$\delta\mathrm{sign}(\cdot)$ with saturation constant $\delta > 0$.
$\delta_\omega(\delta_v)$	Saturation constant for frequency (voltage).
$\delta_p(\delta_q)$	Saturation constant for active (reactive) power.
$a \sim b$	If and only if $a_i \sim b_i$, $\forall i$ for vectors $a, b \in R^N$, and the relationship '$\sim$' can be '$\geq$', '$\leq$', '$>$', and '$<$'.
$|\hat{x}|$	$(|x_1|,\cdots,|x_N|)^T$ for any vector $x \in R^N$.

I. INTRODUCTION

MICROGRIDS are low voltage power networks comprised of distributed generators (DGs), energy storages systems and loads that can operate in either grid-connected or islanded mode [1], [2]. The main task of MGs is to maintain its own voltage and frequency to certain reference values as well as re-dispatch the active and reactive power among all DGs. The basic control strategy for MGs is the hierarchical control [3], including primary control (droop control, maintaining voltage/frequency stability subsequent to the islanding process) [4], [5], secondary control (compensating the voltage/frequency derivations caused by primary control) [6], [7], and tertiary control (optimal operation in both operating modes and power flow control in grid-tied mode) [8].

The conventional droop mechanics usually suffers from the inherent coupling between frequency and voltage and dependance on output line impedances. The developed voltage-

reactive power droop control still ends up with inaccurate reactive power sharing under non-negligible line impedances [9]. To solve this problem, a modified droop control was proposed [10], where inaccurate reactive power sharing is still observed under strongly non-uniform line impedances. Additionally, the existing secondary control strategies have endeavored from centralized[11,12], decentralized [13]-[16], to the current distributed control [7], [17], [18]. This is partly inspired by the idea of cooperation control for multi-agent systems [19], [20], which allows all DGs to communicate with their neighbors via local communication networks.

Most of the secondary control-related works investigate the frequency/voltage regulation and active power sharing with the asymptotically convergence speed [21]. To accelerate the convergence speed, a finite-time frequency synchronization method and a finite-time approximate consensus strategy were, respectively, proposed in [22] and [23], where the voltage and reactive power control are not considered. Following this line, the finite-time voltage restoration for islanded MGs was studied in [24], through which voltage controller can be designed separately from the frequency control though the accurate reactive power sharing is still not considered.

Up to now, few literatures study the accurate reactive power sharing in MGs with line impedances partly because the traditional droop control is not sufficient to solve such problems [25]. Recently, without relying on the communication between DGs, an enhanced load demand sharing strategy was proposed in [26] by injecting small active power disturbances, sent from a central controller, to estimate the reactive power errors. Then a virtual impedance optimization method was also presented to reduce the reactive power errors [27]. After that, by integrating the communication and the adaptive virtual impedance method, the reactive power sharing accuracy has been further improved [28], even considering the imbalance power case by using a harmonic power sharing scheme [29]. In addition, with the MGs considered to be with line impedances, a novel approach for reactive power sharing was proposed [21], where each DG needs to take the averaged value of all DGs' measured reactive powers as its own nominal state so as to finish the update process. This way, reactive power sharing can be obtained independently from voltage sensing mismatches or line impedances. Another alternative approach is to use the traditional energy function method [30] on the condition of uniform line impedances [31].

This paper investigates the secondary control for islanded MGs and a novel distributed coordination control approach is proposed. The main contributions are three-folds.

1. A finite-time frequency and active power control strategy is proposed to ensure the frequency regulation and active power sharing accuracy within a finite time, which enables the voltage and reactive power control to be achieved in a slow time scale. Compared with the asymptotic convergence schemes [21], [39], [40], this approach can reduce the inherent frequency and voltage coupling in case of non-uniform line impedances to some extent, then the voltage and reactive power control strategy can be designed separately.

2. An observer-based voltage controller involving reactive power constraints is designed to regulate the weighted average voltage of all DGs to their reference and thus, the issue of accurate reactive power sharing in case of strongly non-uniform line impedances can be addressed, which is different from the schemes [22]-[24], [40] that did not consider voltage regulation and/or reactive power sharing.

3. All the designed controllers are equipped with bounded control inputs, which can in turn greatly suppress the general transient overshoot [20], [33], [39]. Moreover, different from [11], [12], [21], a sparse communication network is sufficient to support the proposed scheme, even allowing only one DG to access the reference values. Apart from the plug-and-play capacity, the proposed scheme also possesses high robustness against link failure, time delays, and data drop-out.

The rest of this paper is organized as follows. Section II formulates the distributed cooperative control problem. Two control strategies are designed and analyzed in Section III. Section IV gives the numerical results via a non-parallel configuration MG. Section V concludes this paper.

II. PROBLEM FORMULATION AND PRELIMINARIES

A. Problem Formulation

Consider an islanded MG with N three-phase inverter-based DGs, each DG consists of a prime DC source, a DC/AC inverter, and an Inductance-Capacitance-Inductance (LCL) filter. For the ith DG, the basic internal multiple control loops as well as the primary and secondary control procedure can be drawn in Fig. 1. The abc/dq transformation is considered to decouple active and reactive powers, where the d-axis and q-axis of the reference frame are rotating at the common reference.
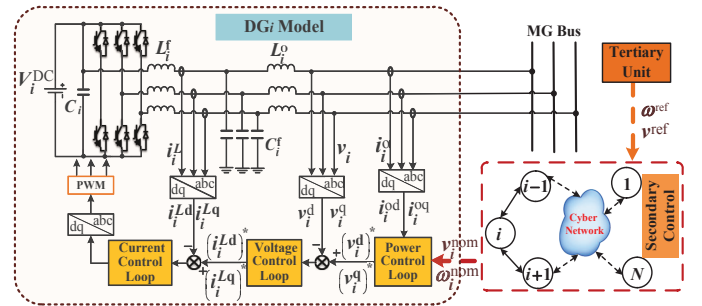
Fig. 1.   The basic control loops for an inverter-based DG.

As seen, the power, voltage, and current control loops (P/V/I inner loops) are employed in DGs. The primary control is implemented during the power control loop with the nominal set points ω_i^{nom} and v_i^{nom}, generated by the secondary control process. With the reference values, $(v_i^{\mathrm{d}})^*$ and $(v_i^{\mathrm{q}})^*$, provided by the power loop, the voltage loop generates the reference values, $(i_i^L\mathrm{d})^*$ and $(i_i^L\mathrm{q})^*$, for the current loop. Then, the current error is calculated and finally used to regulate the output of the inverter by the sinusoidal pulse width modulation (SPWM) mode [1], [7].

The LCL filter locally installed in each DG makes the output impedance highly inductive and dominate any resistive effects, then the droop control law can be given as:

$$\begin{cases} \omega_i = \omega_i^{\mathrm{nom}} - K_i^P P_i, \\ v_i = v_i^{\mathrm{nom}} - K_i^Q Q_i, \end{cases} \tag{1}$$

where the droop coefficients, K_i^P and K_i^Q, are generally selected based on the output power ratios, or the formulas, $K_i^P = \Delta\omega/P_{i,\max}$ and $K_i^Q = \Delta v/Q_{i,\max}$ with the maximum acceptable frequency and amplitude output voltage derivations $\Delta\omega$ and Δv [1]. The magnitude $v_i = \sqrt{(v_i^{\mathrm{d}})^2 + (v_i^{\mathrm{q}})^2}$ with the d-axis and q-axis voltages v_i^{d} and v_i^{q}. Since the primary voltage control aligns the voltage magnitude on the d-axis of its reference frame, then for the ith DG, $v_i^{\mathrm{q}} = 0$.

To compensate the voltage/frequency deviations induced by the primary control, the distributed secondary controller is applied. It collects DG_i's own information as well as its neighbors' through the sparse communication network, then updates ω_i^{nom} and v_i^{nom} for the primary control process. Since ω^{ref} and v^{ref} generated by the tertiary unit, are available to a small part of DGs or at least one DG (e.g. DG_1), all the other DGs can access them indirectly by the information exchanges. Thus, the terminal outputs (frequency/voltage) of the ith DG, can be finally regulated to their references.

B. Preliminaries of Communication Network

An MG can be considered as a multi-agent system, where each DG is an *follower-agent*, and the tertiary unit that is responsible for sending reference values to the MG is a *virtual leader-agent*. The communication network can be modeled by a digraph $\mathcal{G}(\mathcal{V}, \mathcal{E}, A)$ with a node set $\mathcal{V} = \{\mathcal{V}_1, \mathcal{V}_2, \cdots, \mathcal{V}_N\}$, a communication link set $\mathcal{E} \subseteq \mathcal{V} \times \mathcal{V}$, and a weighted adjacency matrix $A = (a_{ij})_{N \times N}$. In detail, $a_{ii} = 0$, $a_{ij} \geq 0$, and $a_{ij} > 0$ if and only if the link $(\mathcal{V}_i, \mathcal{V}_j) \in \mathcal{E}$. A weighted digraph $\mathcal{G}(A)$ is detail-balanced (or balanced) in weights if there exist some scalars $\xi_i > 0$ such that $\xi_i a_{ij} = \xi_j a_{ji}$ for all i and j (or $\sum_{j=1}^{N} a_{ij} = \sum_{j=1}^{N} a_{ji}$ for all i) [20]. Particularly, an undirected graph (all links are bidirectional) always satisfies both the detail-balanced and balanced conditions. The set of DG_i's neighbors is given by $N_i = \{\mathcal{V}_j \in \mathcal{V} : (\mathcal{V}_i, \mathcal{V}_j) \in \mathcal{E}\}$. The Laplacian matrix $L = (\ell_{ij})_{N \times N}$ is defined as $\ell_{ij} = -a_{ij}$, $i \neq j$, and $\ell_{ii} = \sum_{k=1}^{N} a_{ik}$ for all i, which satisfies $L\mathbf{1}_N = 0$ with $\mathbf{1}_N = (1, \cdots, 1)^T \in R^N$. A diagraph is said to have *a spanning directed tree* if there is a root node with a directed path from that node to every other node in the graph. A digraph is *strongly connected* if there is a directed path between any two nodes in the graph. Diagonal matrix $B = \mathrm{diag}\{a_{10}, \cdots, a_{N0}\}$ is called the *virtual leader adjacency matrix*, where $a_{i0} > 0$ if follower DG_i is connected to the leader across the link $(\mathcal{V}_0, \mathcal{V}_i)$, otherwise $a_{i0} = 0$.

III. DISTRIBUTED SECONDARY CONTROL SCHEME

The basic control objective is to tune the frequency and voltage magnitude deviations to the reference values. To this end, differentiating equation (1) yields

$$\dot{\omega}_i^{\mathrm{nom}} = \dot{\omega}_i + K_i^P \dot{P}_i = u_i^\omega + K_i^P u_i^p, \qquad (2)$$

$$\dot{v}_i^{\mathrm{nom}} = \dot{v}_i + K_i^Q \dot{Q}_i = u_i^v + K_i^Q u_i^q, \qquad (3)$$

where $u_i^\omega = \dot{\omega}_i$, $u_i^v = \dot{v}_i$, $u_i^p = \dot{P}_i$, $u_i^q = \dot{Q}_i$, are the inputs of frequency, voltage, active power and reactive power, respectively. The nominal set points can be calculated by:

$$\omega_i^{\mathrm{nom}} = \int_{t_0}^{t} u_i^\omega(s) + K_i^P u_i^p(s)\mathrm{d}s, \qquad (4)$$

$$v_i^{\mathrm{nom}} = \int_{t_0}^{t} u_i^v(s) + K_i^Q u_i^q(s)\mathrm{d}s. \qquad (5)$$

The basic droop control law (1) holds with an assumption that the phase angle between the inverter output of each DG and the MG bus voltages is small (see Assumption 2 in [32]), this inspires us to seek alternative solutions so that all phase angles (may be not small enough in practice) decrease to small values as fast as possible to further promote decoupling frequency and voltage. In special, if we can regulate all DGs' frequency within finite time while maintaining the active power sharing, then the voltage regulation and reactive power sharing will be realized in a slow time scale. Thus the inherent coupling can be reduced to some extent, and the frequency and voltage controllers can be designed separately. Moreover, in order to obtain the accuracy reactive power sharing in MGs with line impedances, a compromise strategy will be designed such that the weighted average value of all DGs' output voltages converge to the desired reference value.

In view of this, the basic control objectives is to design controllers, u_i^ω, u_i^p, u_i^v, and u_i^q, so as to regulate the nominal set-points, v_i^{nom} and ω_i^{nom}, in (4)-(5) such that:

1. All DGs' frequency regulation and accurate active power sharing can be achieved within finite time, i.e.,

$$\lim_{t \to t_\omega^*} \left|\omega_i(t) - \omega^{\mathrm{ref}}\right| = 0, \omega_i(t) = \omega^{\mathrm{ref}}, \forall t \geq t_\omega^*, \qquad (6)$$

$$\begin{cases} \lim_{t \to t_p^*} |P_i/P_{i,\max} - P_j/P_{j,\max}| = 0, \forall i \neq j, \\ P_i/P_{i,\max} = P_j/P_{j,\max}, \forall t \geq t_p^*, \end{cases} \qquad (7)$$

for some finite convergence time (settling time) $t_\omega^*, t_p^* \geq t_0$.

2. The weighted average value of all DGs' voltages can be regulated to their reference value asymptotically while maintaining the accurate reactive power sharing, i.e.,

$$\lim_{t \to +\infty} \left|\sum_{i=1}^{N} \mu_i v_i(t) - v^{\mathrm{ref}}\right| = 0, \qquad (8)$$

$$\lim_{t \to +\infty} |Q_i/Q_{i,\max} - Q_j/Q_{j,\max}| = 0, \forall i \neq j, \qquad (9)$$

where $\mu = (\mu_1, \cdots, \mu_N)^T$ is the normalized positive weighting factors that will be given later.

A. Finite time frequency regulation and active power sharing

The global error of frequency and active power for DG_i across the networks, $\mathcal{G}^\omega$ and $\mathcal{G}^p$, can be calculated as

$$\begin{cases} e_i^\omega = \sum_{j \in N_i^\omega} a_{ij}^\omega (\omega_j - \omega_i) + b_i^\omega (\omega^{\mathrm{ref}} - \omega_i), \\ e_i^p = \sum_{j \in N_i^p} a_{ij}^p (P_j/P_{j,\max} - P_i/P_{i,\max}), \end{cases} \qquad (10)$$

where $A^\omega = (a_{ij}^\omega)_{N \times N}$, $A^p = (a_{ij}^p)_{N \times N}$, and $B^\omega = \mathrm{diag}\{b_1^\omega, \cdots, b_N^\omega\}$ with $b_i^\omega \geq 0$ is the leader adjacency matrix of frequency. DG_i can access ω^{ref} if and only if $b_i^\omega > 0$. Here, we need only one nonzero b_i^ω.

To achieve finite time frequency regulation and active power sharing, we adopt the combination technique of sign function and fractional power integrator [20], [33], [34], to construct controllers. Moreover, we also equip the controllers with bounded control inputs by injecting saturation constraints [20], [33], to further avoid the transient overshoot and thus

guarantee the steady-state stability of the system. Based on this, we design the following controllers:

$$
\begin{cases}
u_i^\omega = \mathrm{sat}_{\delta_\omega}\left[k\,\mathrm{sig}\left(e_i^\omega\right)^{\frac{1+\alpha}{2}}\right] + \hat{u}_i, \\
\dot{\hat{u}}_i = \mathrm{sat}_{\delta_\omega}\left[\gamma\,\mathrm{sig}\left(e_i^\omega\right)^\alpha\right], \ i = 1, \cdots, N,
\end{cases}
\tag{11}
$$

$$
u_i^p = P_{i,\max}\mathrm{sat}_{\delta_p}[k\,\mathrm{sig}(e_i^p)^\alpha + \gamma e_i^p], \ i = 1, \cdots, N, \tag{12}
$$

where $k, \gamma > 0$ are the control gains, $0 < \alpha < 1$ is the fractional power constant for finite time integrators, and δ_ω, δ_p are respectively the saturation constants for frequency and active power control inputs.

By the detailed derivation process for the finite time stability given in Appendix-B, we obtain the following conclusion.

If $\mathcal{G}^p$ and the detail-balanced digraph $\mathcal{G}^\omega$, respectively, contains a spanning tree, then the droop control law (2) with secondary frequency and active power control inputs, (11) and (12), can guide all DGs' frequencies to their reference values in a finite time while maintaining the active power sharing accuracy provided that the frequency reference ω^{ref} is available to at least one DG.

Remark 1: The state errors given in (10) allow each DG to exchange measurements only with its neighbors, then the required information is not global but adjacent for each DG. Thus, a low band-width sparse communication manner is sufficient to support this requirement, which is much useful for the MGs containing a large number of DGs.

Remark 2: Different gains k and γ may result in different convergence speeds, but the consequent transient overshoot is still undesirable, especially for the high frequent oscillation near the equilibrium [20], [33]. Since the saturation constraint is an effective solution to overcome this problem, then apart from (11) and (12), the voltage and reactive power controllers (13) and (20) will also be equipped with bounded inputs.

Remark 3: As derived in Appendix-B, the final frequency and active power convergence times, t_ω^* and t_p^*, are influenced by both of the fractional power parameter α and the initial state errors. In practice, we can predict the state errors so as to activate the proposed secondary control scheme by using event trigger mechanism once the state errors increase beyond a certain acceptable range [8]. Moreover, by the main proof given in Appendix-B, we conclude that there is no strict constraints on the parameters k and γ, and the control performance can be realized if only we set $k > 0$, $\gamma > 0$, and $0 < \alpha < 1$. In addition, the final convergence time can be further shortened by selecting the fractional power parameter $\alpha \in (0, 1)$ appropriately. As a special case, if we take $\alpha = 1$, then the controllers (11-12) become the general *asymptotic distributed secondary control* (ADSC) schemes [7], [21].

Remark 4: Due to the implementation of secondary frequency control, the original distribution pattern of the active powers generated by the primary control principle may be disturbed [7]. To further ensure the active power sharing be achieved with a faster convergence speed (with respect to voltage regulation and reactive power sharing), we design the finite time active power controller (12).

B. Voltage regulation and accurate reactive power sharing

In small-scale MGs, the low ratings of DGs, small electrical distances between units, and the lack of static compensation requires an accurate reactive power sharing among DGs to prevent overloading [35]. To reach a compromise between accurate reactive power sharing and voltage regulation [36], we design an observer-based voltage control strategy involving reactive power constraints so as to regulate the weighted average value of all DGs' voltages to the reference value while maintaining the reactive power sharing accuracy.

The main idea is to firstly estimate each DG's voltage, v_i, by using a consensus-based algorithm, and then pin the obtained estimated value, $\hat{v}_i$, of each DG to the desired reference value, v^{ref}, asymptotically by using a leader-follower-based pinning control algorithm [20]. Since the consensus-based algorithm enables the estimated voltage, $\hat{v}_i$, to converge to a weighted average value of all DGs' voltages, $\sum_{i=1}^N \mu_i v_i$, then the global voltage regulation can be finally guaranteed.

1) Voltage observer design: Firstly, assume DG$_i$'s observer receives its neighbors' observations $\hat{v}_{j\in N_i}$, and updates its own observation $\hat{v}_i$ by processing the neighbors' estimates and the local voltage measurement v_i as

$$
\hat{v}_i(t) = v_i(t_0) + \int_{t_0}^t \mathrm{sat}_{\delta_v}[\dot{v}_i(\tau) + \sum_{j \in N_i^v} a_{ij}^v\left(\hat{v}_j(\tau) - \hat{v}_i(\tau)\right)]\mathrm{d}\tau,
\tag{13}
$$

where $A^v = (a_{ij}^v)_{N\times N}$ and δ_v is voltage saturation constant.

Since any voltage variation v_i at DG$_i$ will directly steer its observation $\hat{v}_i$ to immediately responds and thereby affects all other observations by observer (13), we then need to analyze the stability of (13). Differentiating it yields

$$
\dot{\hat{v}}_i(t) = \mathrm{sat}_{\delta_v}[\dot{v}_i(t) + \sum\nolimits_{j \in N_i^v} a_{ij}^v\left(\hat{v}_j(t) - \hat{v}_i(t)\right)]. \tag{14}
$$

Let $\hat{v} = (\hat{v}_1, \cdots, \hat{v}_N)^T$, $v = (v_1, \cdots, v_N)^T$, $L^v = (\ell_{ij}^v)_{N\times N}$ (Laplacian matrix corresponding to A^v), the global observer dynamic can be formulated as

$$
\dot{\hat{v}}(t) = \phi_{\delta_v}\left[\dot{v}(t) - L^v\hat{v}(t)\right], \tag{15}
$$

where $\phi_{\delta_v}(\dot{v} - L^v\hat{v}) = (z_1, \cdots, z_N)^T$ with $z_i = \mathrm{sat}_{\delta_v}(\dot{v}_i - \sum_{j \in N_i^v} \ell_{ij}^v)$. Let $\otimes$ be the kronecker product, by the similar technology given in Appendix-A, we yield the set

$$
M = \{\hat{v} : -\delta_v \otimes 1_N \leq \dot{v} - L^v\hat{v} \leq \delta_v \otimes 1_N\}
$$

is positive invariant [36] for system (15), and any trajectories of (15) starting outside of M will finally enter M. Then, take $\hat{v} \in M$, system (15) can be reduced as

$$
\dot{\hat{v}}(t) = \dot{v}(t) - L^v\hat{v}(t). \tag{16}
$$

Write (16) in the frequency domain

$$
\hat{V}(s) = s(sI_N + L^v)^{-1}V(s), \tag{17}
$$

where $\hat{V}$ and V are the Laplace transforms of $\hat{v}$ and v, respectively. If $\mathcal{G}^v$ is strongly connected, then L^v is irreducible. By the Nyquist stability criterion, the transfer function $s(sI_N + L^v)^{-1}$ is stable. Moreover, $\sum_{i=1}^N \mu_i v_i$ is an invariant quantity for the positive left eigenvector μ corresponding to

the zero eigenvalue of irreducible matrix L^v [19], this together with the final value theorem [36] gives:

$$\lim_{t\to+\infty} \hat{v}_i(t) = \lim_{t\to+\infty} \sum_{i=1}^{N} \mu_i v_i(t), \ , i=1,\cdots,N. \quad (18)$$

Hence we conclude that if the digraph $\mathcal{G}^v$ is strongly connected, the voltage observer (13) can steer each DG's voltage observations asymptotically converge to the weighted average value of all DGs' actual voltage magnitudes.

Remark 5: The normalized weighted vector μ is determined by L^v corresponding to the strongly connected digraph $\mathcal{G}^v$. As a special case, $\mu = (1/N,\cdots,1/N)^T$ if $\mathcal{G}^v$ is also balanced. Conversely, if μ is pre-specified, then the associated $\mathcal{G}^v$ can be selected (though such a selection is not unique). For example, take $\mu = (1/2, 1/3, 1/6)^T$ with $N = 3$ and the strongly connected $\mathcal{G}^v$ is selected as an Ring-type digraph (i.e, the adjacency matrix A^v only has nonzero weights a_{21}, a_{32}, and a_{13}), then we can obtain the relationship among these nonzero elements as $a_{13} : a_{32} : a_{21} = 2 : 6 : 3$ by $\mu^T L^v = 0$.

2) Voltage and reactive power controller design: The global error of reactive power for DG$_i$ across the sparse communication network, $\mathcal{G}^q$, can be calculated as

$$e_i^q = \sum_{j\in N_i^q} a_{ij}^q (Q_j/Q_{j,\max} - Q_i/Q_{i,\max}), \quad (19)$$

where $A^q = (a_{ij}^q)_{N\times N}$. The voltage and reactive power controllers, u_i^v (involving reactive power constraint e_i^q) and u_i^q, can be designed as

$$\begin{cases} u_i^v = b_i^v(v^{\text{ref}} - \hat{v}_i) + e_i^q, \\ u_i^q = Q_{i,\max}\text{sat}_{\delta_q}(e_i^q), \end{cases} \quad (20)$$

where δ_q is the saturation constant of reactive power input and $B^v = \text{diag}\{b_1^v,\cdots,b_N^v\}$. We also need only one nonzero b_i^v such that DG$_i$ can access v^{ref}.

The distributed controller (3) under inputs (20) with observer (13) will also enable the control objectives (8) and (9) to be achieved asymptotically provided certain conditions are satisfied. We next derive the conditions.

Let $q_i = Q_i/Q_{i,\max}$, representing DG$_i$'s reactive power output ratio, and integrating (13) and (20) yields

$$\begin{cases} \dot{v}_i(t)=\text{sat}_{\delta_v}\left[\sum_{j\in N_i^v} a_{ij}^v(\hat{v}_j - \hat{v}_i)+b_i^v(v^{\text{ref}} - \hat{v}_i) + e_i^q\right], \\ \dot{q}_i(t)=\text{sat}_{\delta_q}(e_i^q), \end{cases}$$
$$\quad (21)$$

Let $\bar{v}_i = \hat{v}_i - v^{\text{ref}}$, $\bar{v} = (\bar{v}_1,\cdots,\bar{v}_N)^T$, $q = (q_1,\cdots,q_N)^T$, $x = -(L^v + B^v)\bar{v} - L^q q$, and $y = -L^q q$, then (21) can be formulated as

$$\begin{cases} \dot{x} = -(L^v + B^v)\phi_{\delta_v}(x) - L^q\phi_{\delta_q}(y), \\ \dot{y} = -L^q\phi_{\delta_q}(y), \end{cases} \quad (22)$$

where $\phi_{\delta_v}(x) = (\text{sat}_{\delta_v}(x_1),\cdots,\text{sat}_{\delta_v}(x_N))^T$, and $\phi_{\delta_q}(y) = (\text{sat}_{\delta_q}(y_1),\cdots,\text{sat}_{\delta_q}(y_N))^T$. System (22) can be reduced to

$$\dot{x} = -(L^v + B^v)x - L^q y, \quad (23)$$

$$\dot{y} = -L^q y, \quad (24)$$

The proof details can be found in Appendix-A. Then, the solution of equation (24) is $y(t) = e^{-L^q}y(0)$. If $\mathcal{G}^q$ is also strongly connected, it follows from Theorem 3 in [19] that

$$\lim_{t\to+\infty} y(t) = w_r w_\ell^T y(0) = -w_r w_\ell^T L^q q(0) = 0, \quad (25)$$

then the steady state of all DGs' output reactive power ratios $q^s(t) \triangleq (q_1^s,\cdots,q_N^s)^T$ satisfies $L^q q^s = 0$. Thus, $q^s \in \text{span}\{1_N\}$ (the subspace spanned by 1_N), and $q_i^s(t) = q_j^s(t)$ for all $i \neq j$, which deduces the control objective (9). Finally, in the steady state, $y(t) = 0$, then (23) is reduced to

$$\dot{x} = -(L^v + B^v)x. \quad (26)$$

By Lemma 4 in [37], $(L^v + B^v)$ is positive stable, which together with the Lyapunov Stability Theory [36] gives that

$$\lim_{t\to+\infty} \left|\hat{v}_i - v^{\text{ref}}\right| = 0. \quad (27)$$

It combines with (18) give the desired objective (8).

We conclude that if $\mathcal{G}^v$ and $\mathcal{G}^q$ are strongly connected, the droop control law (3) with secondary voltage and reactive power control inputs (20) under voltage observer (13) can guide the weighted average value of all DGs' voltage magnitudes exponentially converge to the reference voltage while maintaining the reactive power sharing accuracy provided that the voltage reference v^{ref} is available to at least one DG.
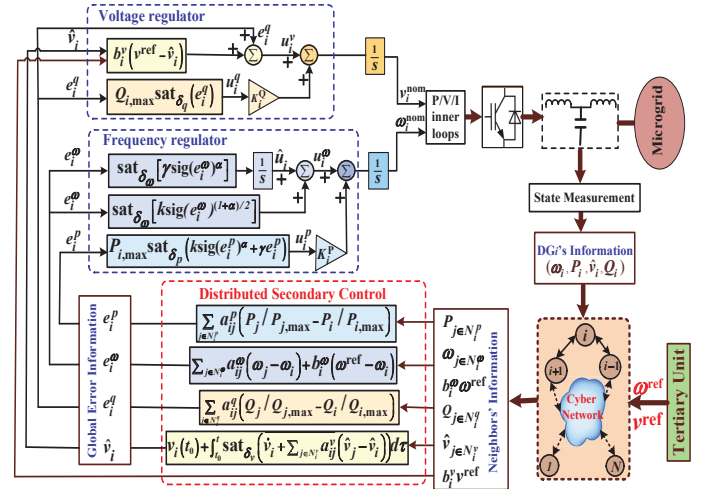

Fig. 2. The block diagram of the proposed PDSC scheme.

The details of the proposed scheme is shown in Fig. 2. As seen, the local secondary controllers can receive its neighbors' measurements, $\{\omega_{j\in N_i^\omega}, P_{j\in N_i^p}, \hat{v}_{j\in N_i^v}, Q_{j\in N_i^q}\}$, and the reference values, $\{b_i^\omega \omega^{\text{ref}}, b_i^v v^{\text{ref}}\}$ (sent from the tertiary unit if DG$_i$ is selected to access the references), through the sparse communication network, $\mathcal{G}^\omega$, $\mathcal{G}^p$, $\mathcal{G}^v$, and $\mathcal{G}^q$. The global error information, $\{e^\omega, e^p, e^q, \hat{v}_i\}$, can be then calculated and fed back to the frequency and voltage regulators. Finally, each DG's own nominal set points, ω_i^{nom} and v_i^{nom}, used in the primary process, can be respectively calculated and updated by the integrator (4) with inputs (11) and (12), and the integrator (5) with input (20) and observer (13). Through such a control framework, the frequency and voltage control possesses different convergence speeds and time scales, which in turn permits us to design these controllers separately. Moreover, the observer-based voltage regulator can be used to deal with the contradiction between voltage regulation and accurate reactive power sharing.

Remark 6: The derived voltage asymptotic convergence is defined in the sense of Lyapunov asymptotic stability [36],

TABLE I
PARAMETER VALUES FOR THE TEST SYSTEM

	DG_1 & DG_3(55 kVA rating)		DG_2 & DG_4(48.3 kVA rating)	
DGs	$V_{DC} : 800V$	$K^P : 7.5 \times 10^{-5}, K^Q : 9 \times 10^{-4}$	$V_{DC} : 680V$	$K^P : 5 \times 10^{-5}, K^Q : 13.5 \times 10^{-4}$
	L_f C_f L_o	2 mH 16 μF 2 mH	L_f C_f L_o	1.95 mH 15 μF 1.95 mH
	current $K_{PI} : 5, 200$	voltage $K_{PID} : 10, 100, 1.5 \times 10^{-3}$	current $K_{PI} : 4, 180$	voltage $K_{PID} : 8, 110, 1.4 \times 10^{-3}$
RL **Lines1-4**	0.64 Ω 1.32 mH	0.51 Ω 1.05 mH	0.58 Ω 1.21 mH	0.61 Ω 1.27 mH
PQ **Loads1-4**	19 kW 19 kVar	18 kW 18 kVar	22kW 22 kVar	17 kW 17 kVar

which ensures that once all DGs' voltages converge to a certain domain around the reference value, they will stay within this domain until some new disturbance occurs. Therefore, the designed controllers can bring all DGs' voltages back once they go out of the acceptable domain.

Remark 7: Different information interactions may possess different communication digraphes, this paper refers to four digraphes $\mathcal{G}^\omega(A^\omega)$, $\mathcal{G}^p(A^p)$, $\mathcal{G}^v(A^v)$, $\mathcal{G}^q(A^q)$, related to the cyber-networks of frequency, active power, voltage, and reactive power, respectively. We also aim to derive the associated weakest connectivity requirements because the results will be beneficial for the network designer to build appropriate redundant network. However, since a strongly connected digraph definitely contains a spanning tree, then we can also choose the four communication digraphes as one uniform *strongly connected digraph* to facilitate the implementation, as used in [8], [15], [18], [24], [25]. Moreover, a connected undirected graph (as a special digraph with all bidirectional links) is always strongly connected, the unified strongly connected digraph can be reduced to a simple *connected undirected graph* condition, as adopted in [38]. In spite of this, all the derived connectivity requirements still allow a sparse communication network and thus, the presented controllers are completely distributed and with low communication costs.

Remark 8: Compared with [21], where each DG needs to average its own reactive power and all the other DGs' to finish the update process, the proposed controller (21) allows different set points for different DGs and, thus, accounts for the non-uniform line impedance effects. Moreover, different from [21], [24], the proposed controllers (11) and (12) guarantee the finite time frequency regulation under sparse communication networks with different weights. Further, compared with [18], where the reference voltage is available to each DG, the controllers (11) and (20) allow only a small part of DGs or even one DG to access the reference values. In addition, different from the finite time frequency and voltage regulation strategy investigated in [22]-[24], the proposed scheme also accounts for the contradiction between precise voltage regulation and reactive power sharing. Finally, all the proposed controllers are with bounded inputs to avoid the transient overshoop, which makes the results more practical.

IV. PERFORMANCE VALIDATION

This section simulates a test system of 380V (per phase RMS), 50Hz (314rad/s) islanded MG (shown in Fig. 3) in
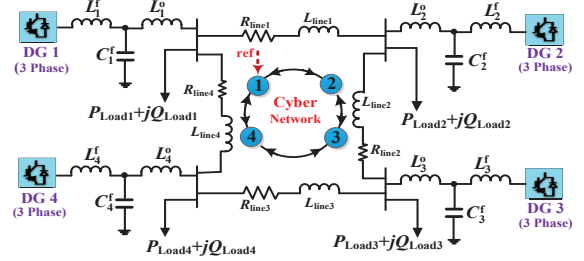

Fig. 3. A single line diagram of the MG test system.

MATLAB/SimPower Systems. The test MG consists of 4 DGs, 4 respective local loads and 4 transmission lines, and the detailed parameters are summarized in Table I.

According to Remark 7, we consider the Ring shaped network (shown in Fig. 3) with each communication weight 1 as the unified digraph. Then the associated adjacency matrices are $A^\omega = A^v = A^p = A^q = [0, 1, 0, 1; 1, 0, 1, 0; 0, 1, 0, 1; 1, 0, 1, 0]$. We assume only DG_1 can access the reference values, then the leader adjacency matrices are $B^\omega = B^v = \text{diag}\{1, 0, 0, 0\}$. Clearly, the selected digraph is detail-balanced. The voltage weighted vector μ corresponding to L^v can be calculated as $\mu = (0.25, 0.25, 0.25, 0.25)^T$. We take $k = 3$, $\gamma = 1$, and $\alpha = 0.5$. Finally, the saturation input constants, δ_ω, δ_p, δ_v, and δ_q, can be selected based on their physical meaning. Intuitively, small saturation constants may lead to slow convergence speed but good transient response, thus we need to make a trade-off between the two performance requirements. Here we take $\delta_\omega = 2$, $\delta_v = 10$, and $\delta_p = \delta_q = 1.5$.

The simulation results will be performed in six scenarios: 1) load variation, 2) plug and play capability, 3) communication topology change, 4) link failure, 5) communication delays, and 6) data drop-out. Some comparisons among the *proposed distributed secondary control* (PDSC) scheme, the general *asymptotic distributed secondary control* (ADSC) scheme, and the traditional *asymptotic centralized secondary control* (ACSC) scheme will be given under the same scenario.

A. Load Variation

The effectiveness of the proposed PDSC scheme, especially for the voltage observer, bounded inputs, the robustness to the large R/X line impedances, and the step response performance, will be verified in case of load changes.

(a1) Frequency response.   (b1) Voltage response.   (c1) Active power outputs.   (d1) Reactive power outputs.

(a2) Frequency inputs.   (b2) Voltage inputs.   (c2) Active power inputs.   (d2) Reactive power inputs.
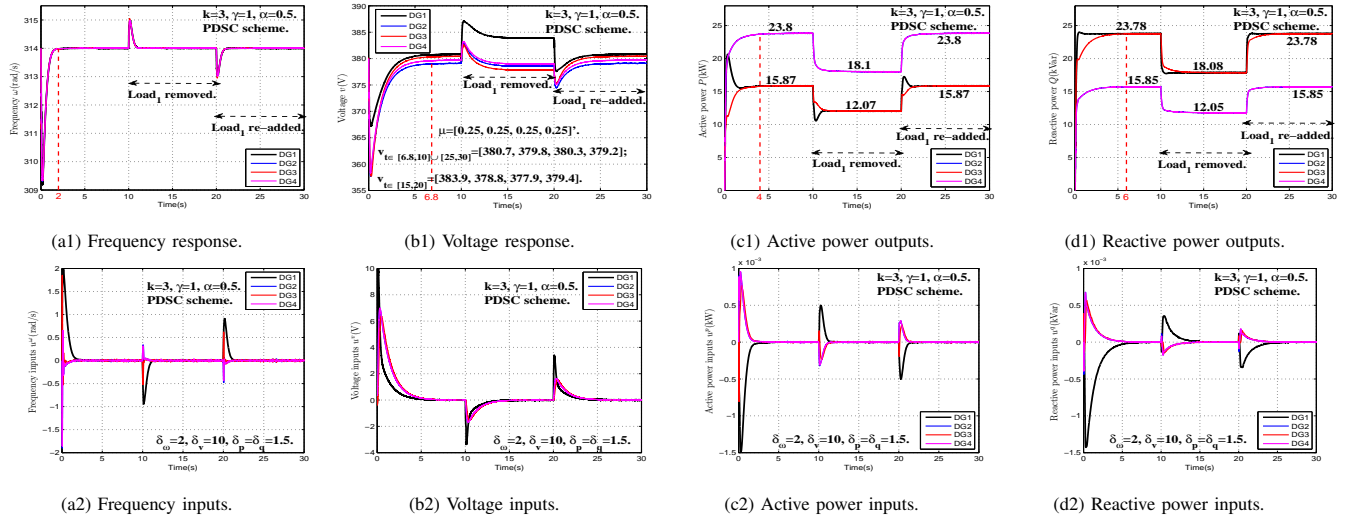
Fig. 4.   State and control input evolutions under the PDSC scheme in case of load variation (the-red dashed lines show the convergence time). (a1) Frequency response. (b1) Voltage response. (c1) Active power outputs. (d1) Reactive power outputs. (a2) Frequency inputs. (b2) Voltage inputs. (c2) Active power inputs. (d2) Reactive power inputs.
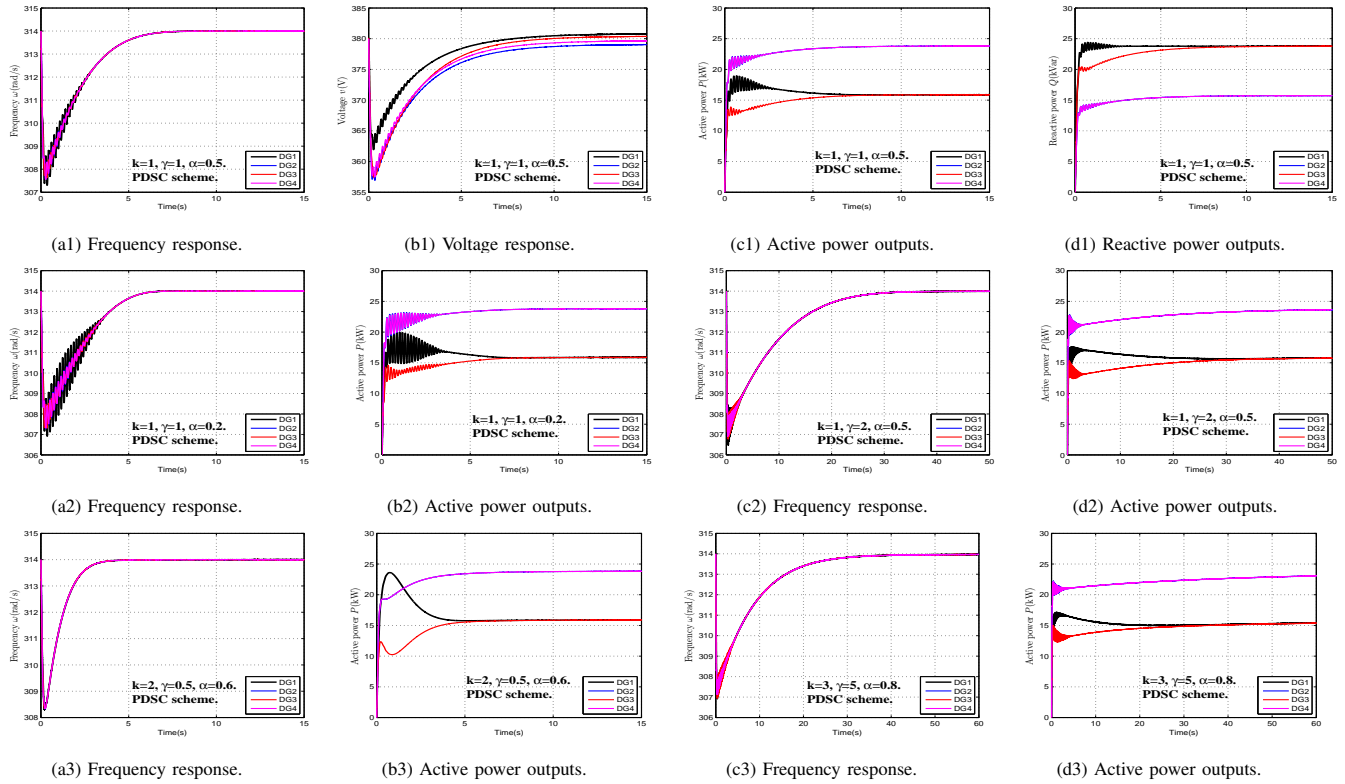

(a1) Frequency response.   (b1) Voltage response.   (c1) Active power outputs.   (d1) Reactive power outputs.

(a2) Frequency response.   (b2) Active power outputs.   (c2) Frequency response.   (d2) Active power outputs.

(a3) Frequency response.   (b3) Active power outputs.   (c3) Frequency response.   (d3) Active power outputs.

Fig. 5.   State evolutions under the PDSC scheme with different control parameters: k, γ, and α. (a1), (a2), (c2), (a3), and (c3) Frequency response. (b1) Voltage response. (c1), (b2), (d2), (b3), and (d3) Active power outputs. (d1) Reactive power outputs.

(a) Frequency response.   (b) Voltage response.   (c) Active power outputs.   (d) Reactive power outputs.
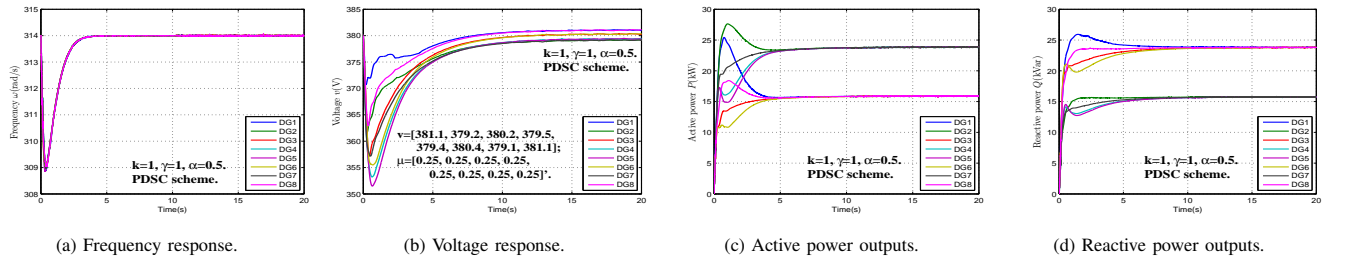
Fig. 6.   State evolutions under the PDSC scheme in case of MG with 8 DGs, 8 local loads, and 8 transmission lines, where $DG_{5,7}$ and $DG_{6,8}$ respectively have the same parameters as those of $DG_{2,4}$ and $DG_{1,3}$, and the whole physical and cyber networks are also Ring shaped (as shown in Fig. 3). (a) Frequency response. (b) Voltage response. (c) Active power outputs. (d) Reactive power outputs.

1) General performance assessment: The control performance in case of load variation are studied in Fig. 4. The test MG begins to operate in islanded mode at $t = 0$s with local Loads 1-4 and the PDSC scheme is activated simultaneously. As seen, the total load increases after $t = 0$s, the frequency and voltage synchronization to the nominal references (314 rad/s and 380V) are then lost. The PDSC scheme is then returns all frequencies to 314 rad/s within 2s and keeps active power sharing accuracy within 4s. After $t = 6.8$s, all DGs' voltages begin to stabilize near 380V, while the reactive power sharing accuracy is achieved within 6s. When local Load$_1$ (19kW$+j$19kVar, locally installed in DG$_1$) is removed at $t = 10$s and re-added (installed in DG$_1$ again) at $t = 20$s, the similar transient response and excellent steady performance can be observed in Fig. 4(a1)-(d1), the associated bounded control inputs are also shown in Fig. 4(a2)-(d2). Fig. 5 shows the control performance with different parameters k, γ, and α. As seen, there is no strict constraints on the selection of these parameters, although different values may lead to different convergence speeds. For large size MGs, we simulate a MG containing 8 DGs in Fig. 6. Although the final convergence time increases, compared with Fig. 4, the total control objective can still be achieved.

achieved. However, for the case of unbounded control inputs (see Fig. 8(c)-(d)), more transient overshoot for the frequency and active power control (see Fig. 8(a)-(b)) can be observed by comparing Fig. 4(a1) and (c1) with Fig. 8(a,b).

4) ADSC scheme with or without voltage observer: By setting $\alpha = 1$, we simulate the general ADSC scheme without and with voltage observer (13) in Figs. 9 and 10, respectively. As seen in Fig. 9, the accurate reactive power sharing could not be achieved due to the inherent contradiction between voltage regulation and reactive power sharing. Moreover, comparing Fig. 10 with Fig. 4(a1)-(d1), the convergence time of ω, v, P, and Q in Fig. 10 are, respectively, 8s, 10s, 11s, and 9s, while those in Fig. 4 are, respectively, 2s, 4s, 6s, and 6.8s, thus the PDSC scheme possesses faster convergence speed than the general ADSC scheme.

5) PDSC vs ADSC with large R/X line impedances: We simulate the PDSC and the general ADSC schemes in case of large R/X line impedances in Fig. 11. The four line parameters are, respectively, set as $0.96\Omega + j0.41\Omega$, $0.76\Omega + j0.33\Omega$, $0.87\Omega + j0.38\Omega$, and $0.91\Omega + j0.4\Omega$. As seen, the excellent control performance for the PDSC scheme (Fig. 11(a)-(b)) can be observed. This is because that the proposed finite time control framework can naturally lead to a faster convergence time so as to effectively distinguish a slower convergence time scale of voltage and reactive power, thereby decoupling the voltage and frequency control to some extent.
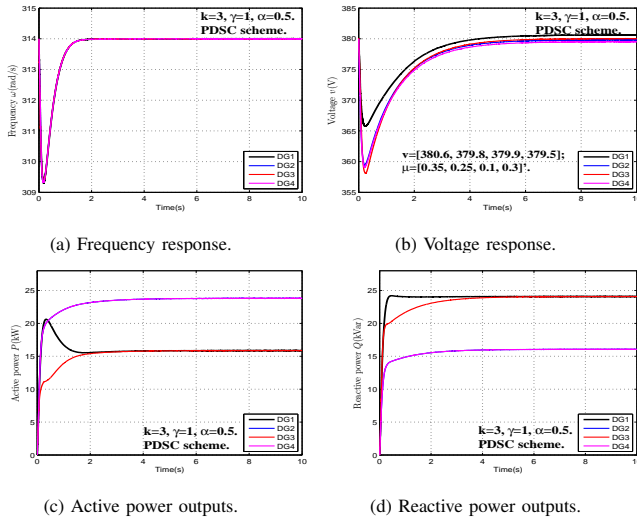

Fig. 7. State evolutions under the proposed PDSC scheme with pre-specified weighted vector $\mu = (0.35, 0.25, 0.1, 0.3)^T$ (The associated adjacency matrix for digraph $\mathcal{G}^v$ is designed as A^v with $a_{21} = 1.2$, $a_{32} = 3$, $a_{43} = 1$, $a_{14} = 0.86$, and $a_{ij} = 0$ for other i and js). (a) Frequency response. (b) Voltage response. (c) Active power outputs. (d) Reactive power outputs.
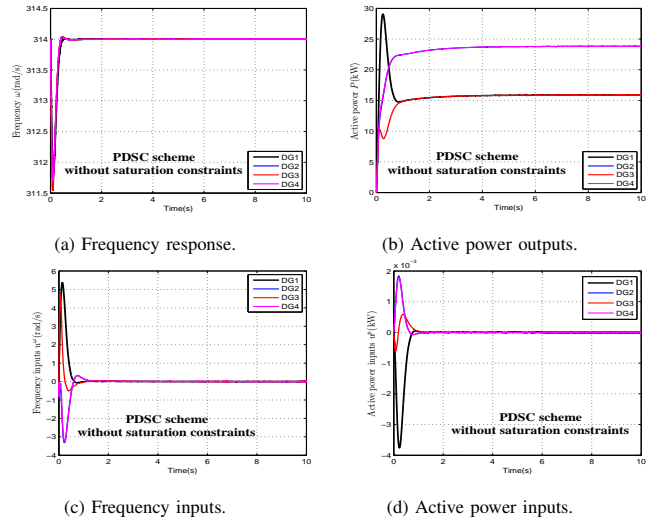

Fig. 8. State and control input evolutions under the proposed PDSC scheme without using the saturation constraint control. (a) Frequency response. (b) Active power outputs. (c) Frequency inputs. (d) Active power inputs.

2) Test for voltage weighted vector μ: As seen in Fig. 4(b1), for $t \in [6.8, 10]$s, the weighted average value of all DGs' voltages can be calculated as $\mu^T v = 380$V. Furthermore, as described in Remark 5, Fig. 7 shows the control performance under a directed communication network $\mathcal{G}^v$ designed by a pre-specified vector μ. As seen, the weighted average voltage in the steady state can be calculated as $\mu^T v = 380$V, which verifies the effectiveness of this selection.

3) Boundedness of the control inputs: Fig. 4(a2)-(d2) shows the control input evolutions of the PDSC scheme. As seen, all the control inputs are bounded by the given saturation constants and finally converge to zero when the steady state is

6) Step response test: To further validate the effectiveness of the PDSC scheme, we compare the response of the established model (state space equation obtained by integrating the secondary control diagram given in Fig. 2 and the multiple control loops given in Fig. 1 with ω^{ref}, v^{ref} being the inputs and ω, v, P, Q being the outputs) with the simulation results in Fig. 12. As seen, all the step response curves fit well.

B. Plug-and-Play Capability

The effectiveness of the plug-and-play capability is analyzed here. The MG containing DGs 1-4 is operating at $t = 0$s with
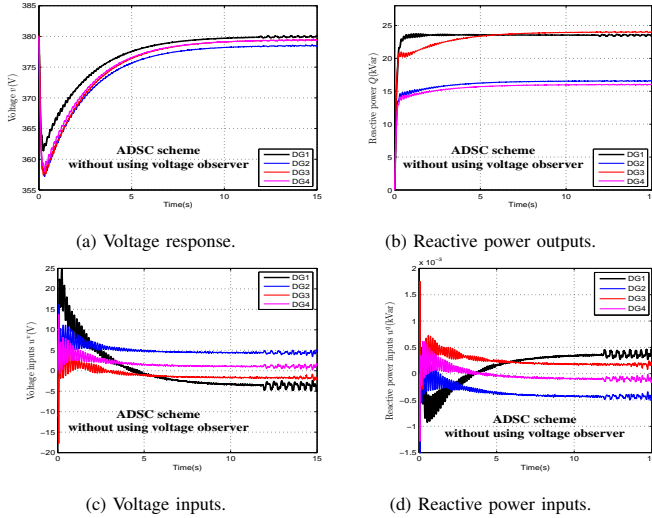
Fig. 9. State and control input evolutions under the general ADSC scheme without using voltage observer. (a) Voltage response. (b) Reactive power outputs. (c) Voltage inputs. (d) Reactive power inputs.

Fig. 11. State evolutions under different control schemes with large R/X line impedances ((a),(b): PDSC scheme; (c),(d): ADSC scheme.). (a) and (c) Voltage response. (b) and (d) Reactive power outputs.

Loads 1-4. Assume DG_5 (with the same parameters as DGs 2 and 4) is plugged in at $t = 5$s (12s for the general ADSC scheme) and DG_4 is plugged out at $t = 10$s (21s for the general ADSC scheme). The associated line impedance is set as $0.62\Omega + j0.4\Omega$. We increase each communication weight in the digraph given in Fig. 3 to 2 in this case. The associated simulations are given in Fig. 13.
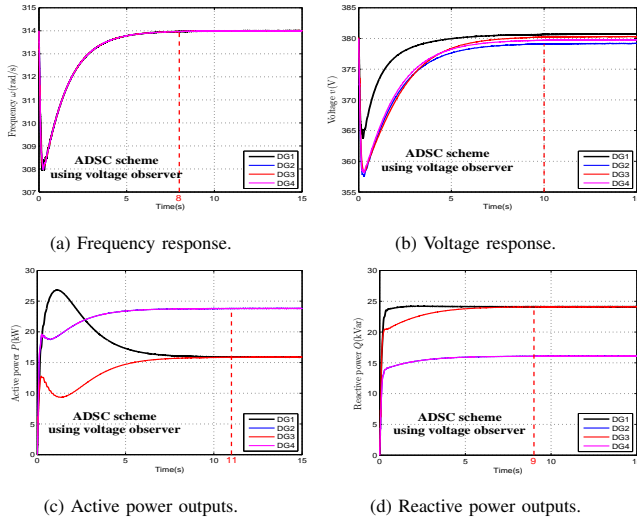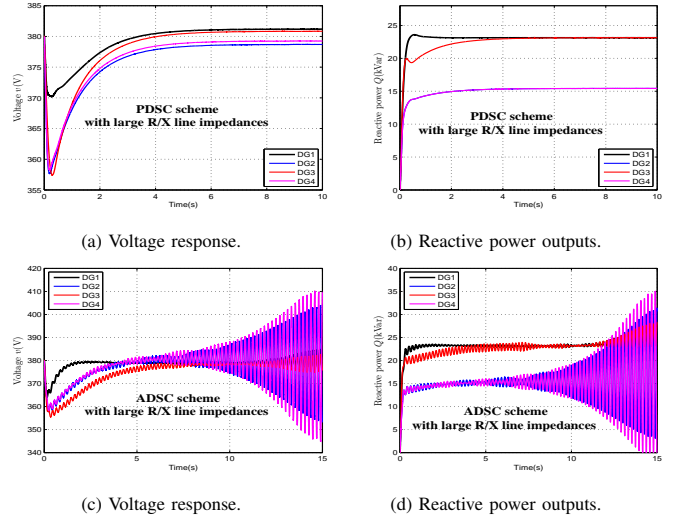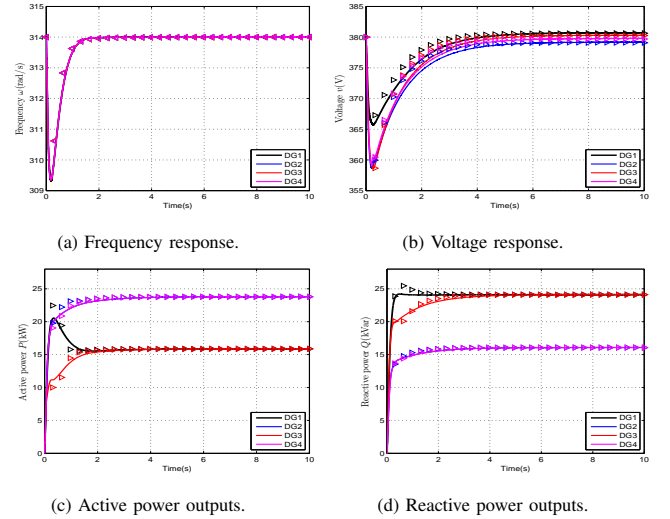

Fig. 10. State evolutions under the general ADSC scheme using voltage observer (the red-dashed lines show the convergence time). (a) Frequency response. (b) Voltage response. (c) Active power outputs. (d) Reactive power outputs.

Once a new DG is authorized to be plugged in the islanded MG, some new communication links will be added. We add links 1-5 (between DGs 1 and 5) and 1-4 with weight 2 for each link when DG_5 is plugged in. As seen in Fig. 13(a1)-(d1), after DG_5 is plugged in at $t = 5$s, the desired control performance can be observed within 3s. When DG_4 is plugged out at $t = 10$s, its states are no longer available. Thus,

Fig. 12. The step response of the controlled system ('▷' represents the response of the state space equations.). (a) Frequency response. (b) Voltage response. (c) Active power outputs. (d) Reactive power outputs.

the controllers average the other DGs' states, and readjust the power output pattern, as shown in Fig. 13(c1) and (d1). Removing DG_4 also implies loss of the links 1-4, 5-4, and 3-4. However, the remaining links still form a connected digraph (see Fig. 3) and, thus, the whole control system is still functional.

Comparing with the state evolutions shown in Fig. 13(a2)-(d2), where the general ADSC scheme is used, the PDSC scheme possesses more excellent transient response and steady-state performance, as shown in Fig. 13 (a1)-(d1).

C. Communication Topology Change

We study the control performance of the PDSC scheme under Full connected, Star shaped, Tree shaped, and Line shaped communication networks in Fig. 14. Comparing the

(a1) Frequency response.   (b1) Voltage response.   (c1) Active power outputs.   (d1) Reactive power outputs.

(a2) Frequency response.   (b2) Voltage response.   (c2) Active power outputs.   (d2) Reactive power outputs.
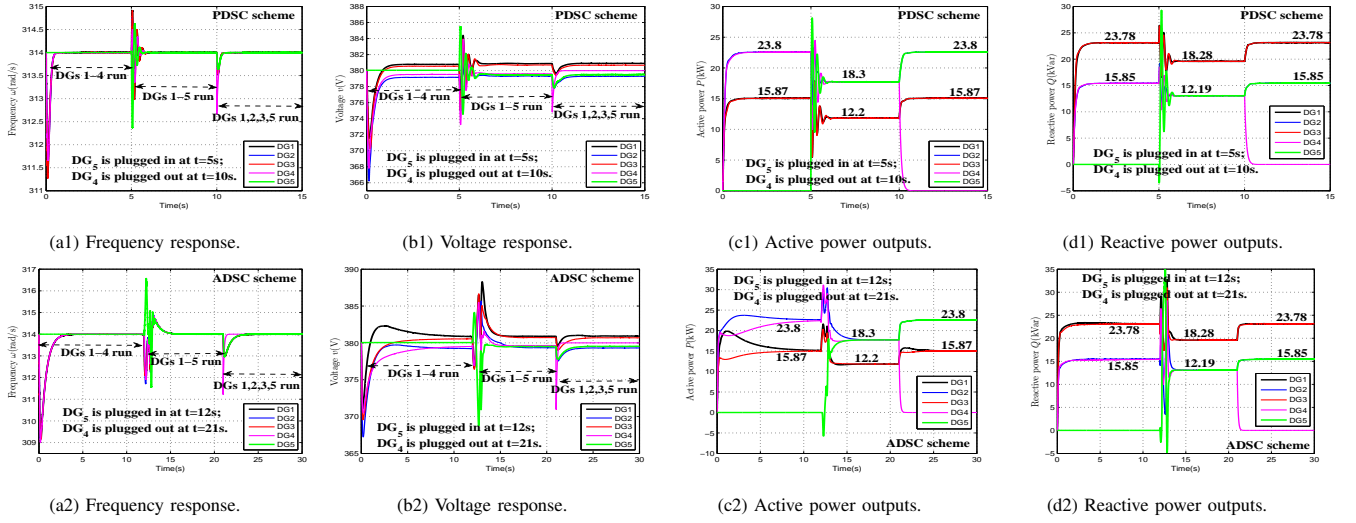
Fig. 13.   State and control input evolutions under different control schemes in case of DG plug-and-play operation. (a1) and (a2) Frequency response. (b1) and (b2) Voltage response. (c1) and (c2) Active power outputs. (d1) and (d2) Reactive power outputs.

(a1) Frequency response.   (b1) Voltage response.   (c1) Active power outputs.   (d1) Reactive power outputs.

(a2) Frequency response.   (b2) Voltage response.   (c2) Active power outputs.   (d2) Reactive power outputs.

(a3) Frequency response.   (b3) Voltage response.   (c3) Active power outputs.   (d3) Reactive power outputs.

(a4) Frequency response.   (b4) Voltage response.   (c4) Active power outputs.   (d4) Reactive power outputs.
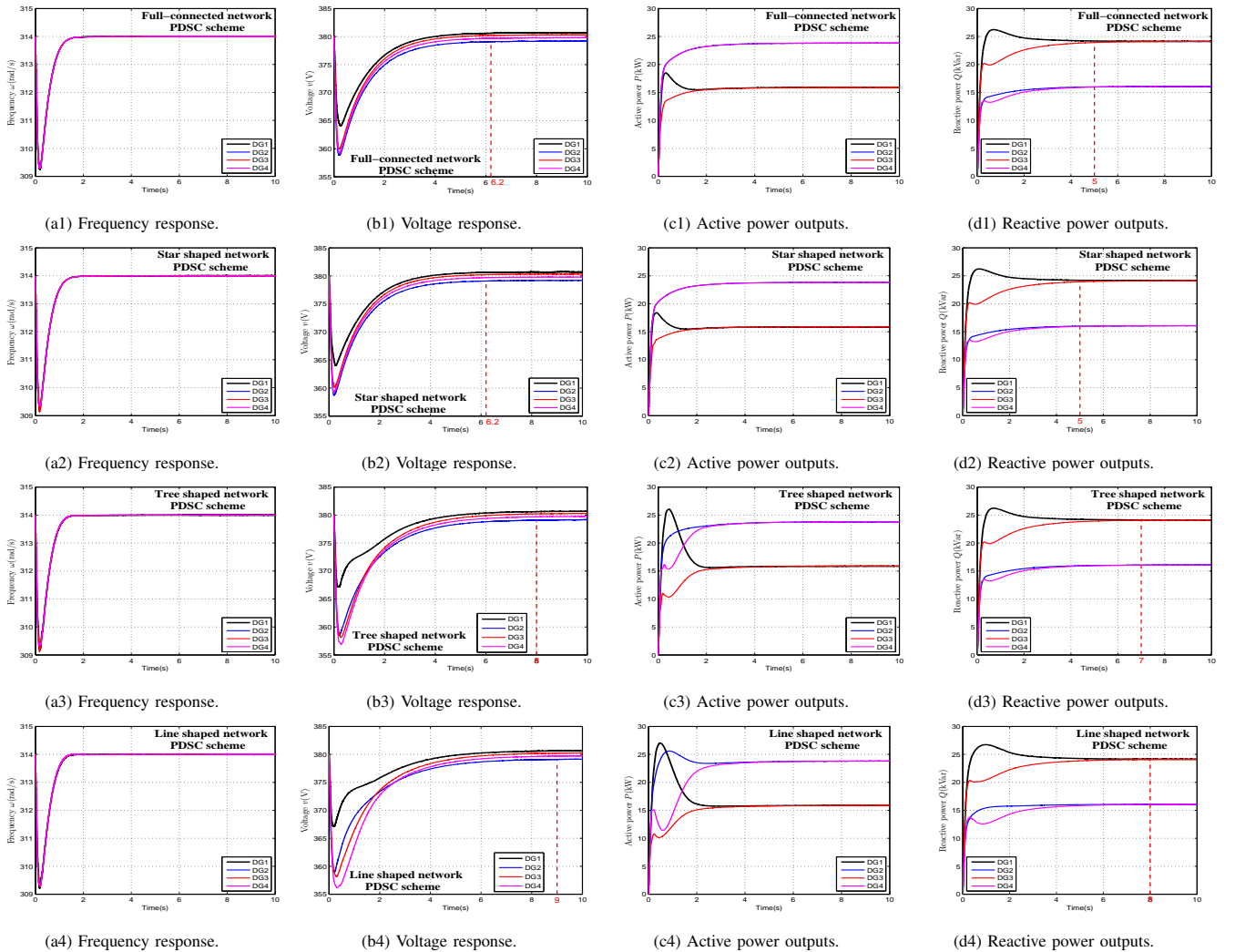
Fig. 14.   State evolutions under different network structures (the red dashed lines show the convergence time). (a1), (a2), (a3), and (a4) Frequency response. (b1), (b2), (b3), and (b4) Voltage response. (c1), (c2), (c3), and (c4) Active power outputs. (d1), (d2), (d3), and (d4) Reactive power outputs.

Different Topos		Full	Star	Ring	Tree	Line
Spectral Radius		0.2087	0.2087	0.1864	0.1392	0.1206
Convergence Time	ω	1.9s	1.9s	2s	2.1s	2.2s
	P	3s	3s	4s	4.5s	5s
	Q	5s	5s	6s	7s	8s
	v	6.2s	6.2s	6.8s	8s	9s

convergence speeds shown in Fig. 14 with that of the Ring shaped network shown in Fig. 4(a1)-(d1), it can be concluded that Full connected and Star shaped networks have the same convergence time which is faster than the others, while the convergence time of Ring shaped network is faster than both Tree shaped and Line shaped ones, and the Line shaped network has the slowest convergence time. This is because that the networks with different topology structures may have different connectivity and then lead to different spectral radius of the coefficient matrices for the controlled system, which determines their own convergence speeds, as calculated in Table II. As seen, there is no significant differences in the convergence times of frequency and active power due to the implementation of finite time control technique, however, this is completely different for the case of voltage and reactive power with asymptotic convergence speeds.

(a1) Voltage response.

(b1) Active power outputs.

(a2) Voltage response.

(b2) Active power outputs.

(a3) Voltage response.
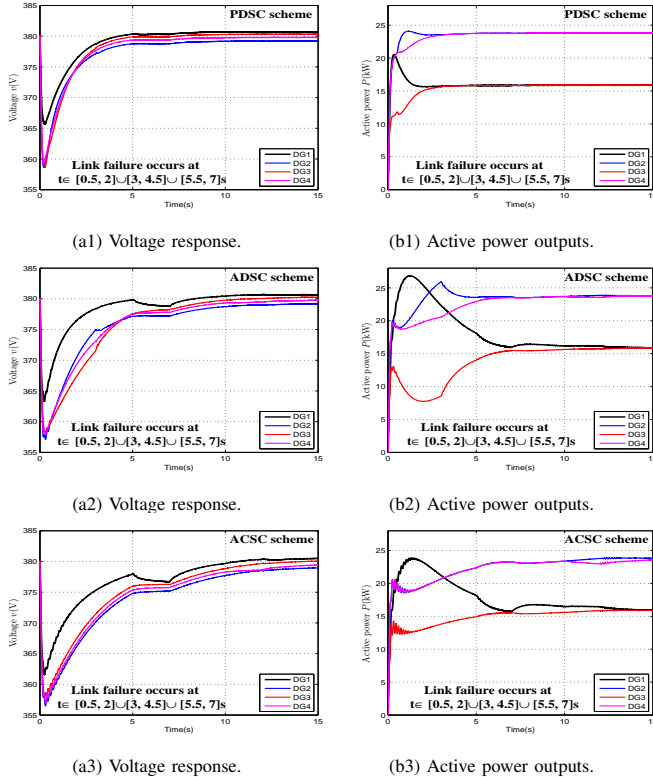
(b3) Active power outputs.

Fig. 15. State evolutions under different control schemes in case of link failure. (a1), (a2), and (a3) Voltage response. (b1), (b2), and (b3) Active power outputs.

D. Link Failure Test

There exists some fallback mode to deal with the extreme case where all communication links fail (e.g., the black start mode [21] or the self-organization strategy [39]), we then analyze the robustness of the PDSC scheme to limited link failure by comparing it with the traditional ADSC and ACSC schemes. In all simulations the links 1-4 and 1-2 are randomly disconnected as $t \in [0.5, 2]$s and $t \in [3, 4.5]$s, respectively. Moreover, the link between the virtual leader-DG_0 to DG_1 is disconnected as $t \in [5.5, 7]$s. As seen, the PDSC scheme (Fig. 15(a1)-(b1)) show the best robustness to link failure. Although the ACSC scheme has the faster convergence time than the ADSC scheme, it still shows poorer transient control performance than the ADSC scheme. In addition, the controlled system is almost free from the impact of link failure (disconnection of link 0-1 as $t \in [5.5, 7]$s) once the secondary control objectives are realized.
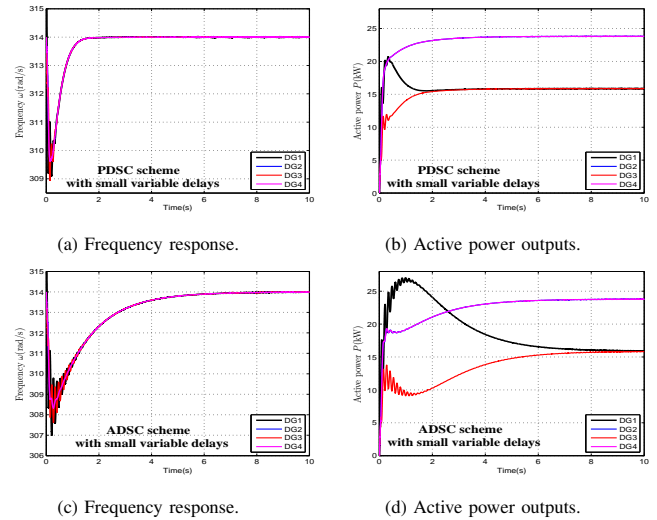

(a) Frequency response.

(b) Active power outputs.

(c) Frequency response.

(d) Active power outputs.

Fig. 16. State evolutions under different control schemes in case of time delays $0.08\sin(10t + \pi/4) + 0.09$. (a) and (c) Frequency response. (b) and (d) Active power outputs.

Based on the robustness, we can make a preliminary attempt on the secure communication problem by timely breaking some links to ensure the information and data security. In practice, all DGs in an MG can be equipped with group communication protocols to ensure the confidentiality, integrity, authenticity and non-repudiation. A key management controller (KMC) located in the tertiary unit can be designed to update the group key periodically and then send the latest common group key to each DG, and all DGs have their own digital signatures authorized by the KMC. Once some incorrect signatures are detected, the KMC will select appropriate links to interrupt so as to ensure the data security and system stability. This will be our future work.

E. Impact of Communication Delays and Data Drop-out

As pointed out in [20], [33], [34], the finite time controllers naturally possess more robustness to the external uncertainties like delays or data drop-out than the general asymptotic
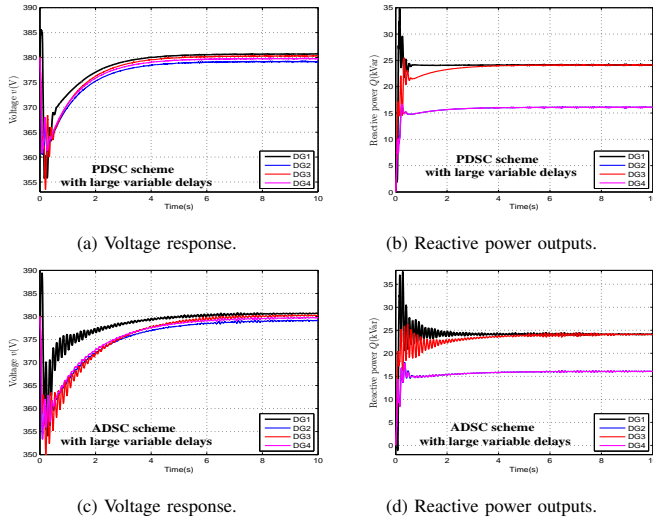
Fig. 17. State evolutions under different control algorithms in case of large time delays $0.1\sin(10t + \pi/4) + 0.15$. (a) and (c) Voltage response. (b) and (d) Reactive power outputs.

Fig. 19. State evolutions under different control schemes in case of data drop-out with packet loss in randomly selected links at each time. (a) and (c) Frequency response. (b) and (d) Active power outputs.
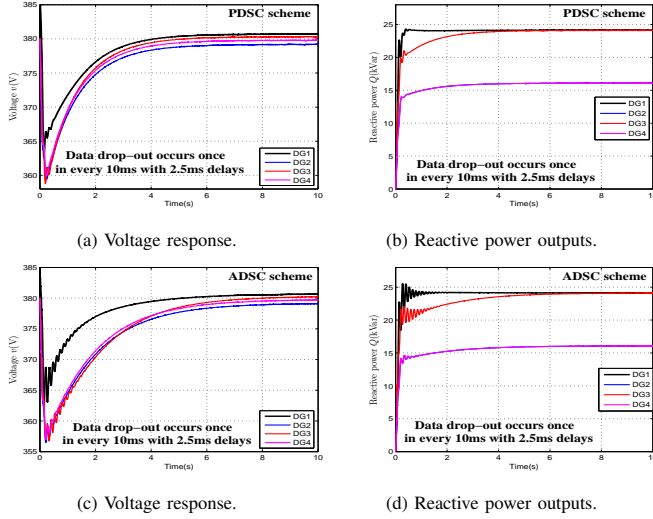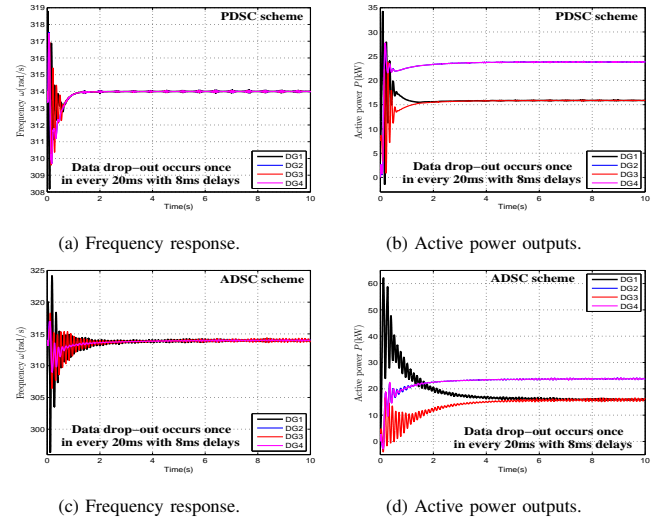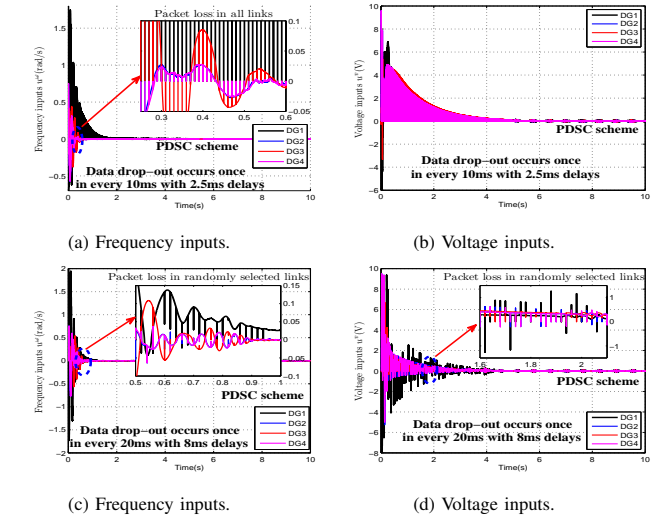

Fig. 18. State evolutions under different control schemes in case of data drop-out with packet loss in all links at each time. (a) and (c) Voltage response. (b) and (d) Reactive power outputs.

Fig. 20. Control input evolutions under the proposed PDSC scheme in case of data drop-out. (a) and (c) Frequency inputs. (b) and (d) Voltage inputs.

controllers, then the impact of communication delays and data drop-out on the PDSC scheme is presented here, by comparing with the traditional ADSC scheme.

Comparing Figs. 16 and 17, it can be seen that both the PDSC and the ADSC schemes are robust to small communication delays, while the proposed scheme shows better robustness in case of large communication delays.

We simulate the results of data drop-out in two situations: i) the data drop-out (packet loss in all links) occurs once in every 10ms, considering 2.5ms communication delays, as shown in Fig. 18; ii) the data drop-out (packet loss in randomly selected links) occurs once in every 20ms, considering 8ms communication delays, as shown in Fig. 19. Fig. 20 presents the associated input evolutions of the PDSC scheme.

As seen in Figs. 18 and 19, the PDSC and the ADSC schemes have an acceptable performance in the first data drop-

out situation, while the ADSC scheme shows a poorer control performance in the second situation. The robustness of the PDSC scheme to the randomly packet loss is verified in Fig. 21, as seen, the whole control performance is not significantly affected after the steady state is realized at $t = 10s$.

V. CONCLUSIONS

Two distributed secondary control strategies involving finite time frequency regulation, weighted average voltage regulation, active and reactive power sharing accuracy have been designed. The proposed finite time controllers ensure the frequency regulation and active power sharing be achieved within a finite time, which enables the voltage regulation and reactive power sharing to be realized in a slow time scale. By this approach, the inherent frequency and voltage coupling can be reduced to some extent. The designed voltage
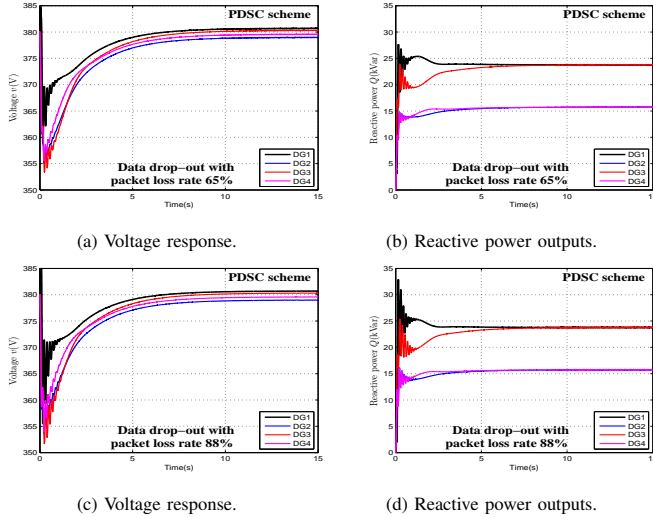
Fig. 21. State evolutions under the proposed PDSC scheme in case of data drop-out. (a) and (c) Voltage response. (b) and (d) Reactive power outputs.

observer can regulate the weighted average value of all DGs' voltages to the reference value, which in turn guarantees the reactive power sharing precisely in large R/X MGs. All the controllers are designed with bounded inputs and implemented under sparse networks, thus the general transient overshoot has been greatly suppressed. Finally, simulation results verified that the proposed scheme can successfully regulate frequency and voltage of the system and accurately share the active and reactive power in islanded MGs with strongly non-uniform line impedances even in the presence of link failure, communication delays, and data packet losses.

APPENDIX

A. Proof for reducing system (22) to system (23)-(24): To facilitate the proof, we let $a_{ij}^q = a_{ij}^v$ and $\delta_q = \delta_v$, however, the general case can be proved similarly.

Define the following sets:

$$\begin{aligned}
\mathcal{A}^+ &= \{(x^T, y^T)^T : x < -\delta_v \otimes 1_N, y \geq \delta_v \otimes 1_N\}, \\
\mathcal{A}^- &= \{(x^T, y^T)^T : x < -\delta_v \otimes 1_N, 0 \leq y < \delta_v \otimes 1_N\}, \\
\mathcal{B}^+ &= \{(x^T, y^T)^T : x \geq \delta_v \otimes 1_N, y \geq \delta_v \otimes 1_N\}, \\
\mathcal{B}_1^- &= \{(x^T, y^T)^T : 0 \leq x < \delta_v \otimes 1_N, y \geq \delta_v \otimes 1_N\}, \\
\mathcal{B}_2^- &= \{(x^T, y^T)^T : -\delta_v \otimes 1_N \leq x \leq 0, y \geq \delta_v \otimes 1_N\}, \\
\mathcal{C} &= \{(x^T, y^T)^T : x \geq \delta_v \otimes 1_N, 0 \leq y < \delta_v \otimes 1_N\}, \\
\mathcal{D} &= \{(x^T, y^T)^T : |\hat{x}| \leq \delta_v \otimes 1_N, |\hat{y}| \leq \delta_v \otimes 1_N\},
\end{aligned}$$

let $\mathcal{A} = \mathcal{A}^+ \cup \mathcal{A}^-$, $\mathcal{B} = \mathcal{B}^+ \cup \mathcal{B}^-$, and $\mathcal{B}^- = \mathcal{B}_1^- \cup \mathcal{B}_2^-$. We prove $\mathcal{D}$ is a positively invariant set for (22), by verifying that no trajectories will leave $\mathcal{D}$ through $\partial \mathcal{D} = \cup_{i=1}^4 \mathcal{D}_i$, where

$$\begin{aligned}
\mathcal{D}_1 &= \{(x^T, y^T)^T : x = -\delta_v \otimes 1_N, |\hat{y}| < \delta_v \otimes 1_N\}, \\
\mathcal{D}_2 &= \{(x^T, y^T)^T : |\hat{x}| < \delta_v \otimes 1_N, y = \delta_v \otimes 1_N\}, \\
\mathcal{D}_3 &= \{(x^T, y^T)^T : x = \delta_v \otimes 1_N, |\hat{y}| < \delta_v \otimes 1_N\}, \\
\mathcal{D}_4 &= \{(x^T, y^T)^T : |\hat{x}| < \delta_v \otimes 1_N, y = -\delta_v \otimes 1_N\}.
\end{aligned}$$

The restrictions of $\dot{x}$ and $\dot{y}$ on $\partial \mathcal{D}$ are given by

$$\begin{aligned}
\dot{x}|_{\mathcal{D}_1} &= (L^v [\delta_v \otimes 1_N \pm |\hat{y}|] + B^v \delta_v \otimes 1_N)|_{\mathcal{D}_1} \geq 0, \\
\dot{y}|_{\mathcal{D}_2} &= -L^v \delta_v \otimes 1_N \leq 0, \\
\dot{x}|_{\mathcal{D}_3} &= -(L^v [\delta_v \otimes 1_N + |\hat{y}|] + B^v \delta_v \otimes 1_N)|_{\mathcal{D}_3} \leq 0, \\
\dot{y}|_{\mathcal{D}_4} &= -L^v(-\delta_v) \otimes 1_N \geq 0.
\end{aligned}$$

Thus no trajectories will leave $\mathcal{D}$ through $\partial \mathcal{D}$. Next, check all trajectories starting in $\mathcal{A}$, $\mathcal{B}$, and $\mathcal{C}$ will enter $\mathcal{D}$ or $\mathcal{B}_2^-$. In fact,

$$\begin{aligned}
\dot{x}|_{\mathcal{A}} &= L^v(\delta_v \otimes 1_N - |\hat{y}||_{\mathcal{A}}) + B^v(\delta_v \otimes 1_N) \geq 0, \\
\dot{y}|_{\mathcal{A}^+ \cup \mathcal{B}} &= -L^v(\delta_v \otimes 1_N) \leq 0, \\
\dot{y}|_{\mathcal{A}^- \cup \mathcal{C}} &= -L^v |\hat{y}||_{\mathcal{A}^- \cup \mathcal{C}} \leq 0, \\
\dot{x}|_{\mathcal{B}^+} &= -(L^v + B^v)(\delta_v \otimes 1_N) - L^v(\delta_v \otimes 1_N) \leq 0, \\
\dot{x}|_{\mathcal{B}_1^-} &= [-L^v(|\hat{x}| + \delta_v \otimes 1_N) - B^v |\hat{x}|]_{\mathcal{B}^-} \leq 0, \\
\dot{x}|_{\mathcal{C}} &= -L^v(\delta_v \otimes 1_N - |\hat{y}||_{\mathcal{C}}) - B^v(\delta_v \otimes 1_N) \leq 0,
\end{aligned}$$

For the set $\mathcal{B}_2^-$, we have $\dot{y}|_{\mathcal{B}_2^-} \leq 0$ and

$$\begin{aligned}
\dot{x}|_{\mathcal{B}_2^-} &= [L^v(|\hat{x}| - \delta_v \otimes 1_N) + B^v |\hat{x}|]|_{\mathcal{B}_2^-} \\
&= \begin{cases} B^v \delta_v \otimes 1_N \geq 0, & \text{if } x = -\delta_v \otimes 1_N, \\ -L^v \delta_v \otimes 1_N \leq 0, & \text{if } x = 0. \end{cases}
\end{aligned}$$

Hence, all trajectories starting in $\mathcal{B}_2^-$ will finally enter $\mathcal{D}$.

Now, let $-\mathcal{A} = \{(x^T, y^T)^T : (-x^T, -y^T)^T \in \mathcal{A}\}$ and define $-\mathcal{B}$, $-\mathcal{C}$ similarly. Then, all the trajectories starting in $-\mathcal{A}$, $-\mathcal{B}$, and $-\mathcal{C}$ will also enter $\mathcal{D}$. This completes the proof.

B. Proof for the stability of system (11)-(12): We derive the main proof here by slightly modifying the associated results given in [20], [33], [34]. Let $\bar{\omega}_i = \omega_i - \omega^{\text{ref}}$, $\bar{\omega} = (\bar{\omega}_1, \cdots, \bar{\omega}_N)^T$, and $x = (x_1, \cdots, x_N)^T$ with $x_i = e_i^\omega$, then $x = (L^\omega + B^\omega)\bar{\omega}$. Moreover, denote $y = (\hat{u}_1, \cdots, \hat{u}_N)^T$, $p = (p_1, \cdots, p_N)^T$ with $p_i = P_i / P_{i,\max}$, and $z = (z_1, \cdots, z_N)^T$ with $z_i = e_i^p$, then $z = L^p p$. By using the similar technique used in Appendix-A, system (11)-(12) can be reduced as

$$\begin{cases} \dot{x} = -k(L^\omega + B^\omega)\text{sig}(x)^{(1+\alpha)/2} + (L^\omega + B^\omega)y, \\ \dot{y} = -\gamma \text{sig}(x)^\alpha, \\ \dot{z} = -k\text{sig}(z)^\alpha - \gamma L^p z. \end{cases}$$

Now take the Lyapunov candidate as $E = E_1 + E_2$ with

$$\begin{aligned}
E_1 &= \gamma(|\hat{x}|^{(1+\alpha)/2})\text{diag}(\sigma^\omega)(|\hat{x}|^{(1+\alpha)/2}) \\
&\quad + \tfrac{1+\alpha}{2} y^T \text{diag}(\sigma^\omega)(L^\omega + B^\omega)y, \\
E_2 &= \tfrac{k}{1+\alpha}(|\hat{z}|^{(1+\alpha)/2})\text{diag}(\sigma^p)(|\hat{z}|^{(1+\alpha)/2}) + \tfrac{\gamma}{2} z^T z,
\end{aligned}$$

where $\sigma^\omega = (\sigma_1^\omega, \cdots, \sigma_N^\omega)^T$ is the positive vector satisfying $(\sigma^\omega)^T L^\omega = (L^\omega)^T \sigma^\omega$ for $\mathcal{G}^\omega$, and $\sigma^p = (\sigma_1^p, \cdots, \sigma_N^p)^T$ is the positive left eigenvector for the zero eigenvalue of L^p corresponding to $\mathcal{G}^p$. By calculation,

$$\begin{aligned}
\dot{E} &\leq -c_1 [E_1(x, y)]^{(1+3\alpha)/(2+2\alpha)} \\
&\quad - c_2 [E_2(z)]^{(2\alpha)/(1+\alpha)} \leq 0,
\end{aligned}$$

where c_1 and c_2 are the positive constants related to E_1 and E_2, respectively. For the case of $\dot{E} = 0$, we yield $(x^T, y^T, z^T)^T = (0, 0, 0)^T$. Since $x = (L^\omega + B^\omega)\bar{\omega}$ with the positive stable matrix $L^\omega + B^\omega$, then $\bar{\omega} = 0$ and thus $\omega_1 = \cdots \omega_N = \omega^{\text{ref}}$. Moreover, since $z = -L^p p$ with $\text{rank}(L^p) = N - 1$ due to the strongly connectivity of $\mathcal{G}^p$, $z = 0$ implies that $p_1 = \cdots = p_N$ and thus $P_1 / P_{1,\max} = \cdots = P_N / P_{N,\max}$. Therefore, the finite time frequency and

active power control problem can be solved within the settling time $t^* = \max\{t^*_\omega, t^*_p\}$ with

$$
\begin{cases}
t^*_\omega = \frac{2(1+\alpha)}{c_1(1-\alpha)}[E_1(e^\omega(0))]^{\frac{1-\alpha}{2(1+\alpha)}}, \\
t^*_p = \frac{1+\alpha}{c_2(1-\alpha)}[E_2(e^p(0))]^{\frac{1-\alpha}{1+\alpha}},
\end{cases}
$$

where $e^\omega = (e^\omega_1, \cdots, e^\omega_N)^T$ and $e^p = (e^p_1, \cdots, e^p_N)^T$. For the general case where $\mathcal{G}^p$ contains a spanning tree, the finite time stability can still be proved similarly.

REFERENCES

[1] N. Pogaku, M. Prodanovic, and T. C. Green, "Modeling, analysis and testing of autonomous operation of an inverter-based microgrid," *IEEE Trans. Power Electron.*, vol. 22, no. 2, pp. 613-625, Mar. 2007.

[2] H. Han, X. Hou, J. Yang, J. Wu, M. Su, and J. M. Guerrero, "Review of power sharing control strategies for islanding operation of ac microgrids," *IEEE Trans. Smart Grid*, vol.7, no.1, pp. 200-215, Jan. 2016.

[3] J. M. Guerrero, J. C. Vasquez, J. Matas, L. G. Vicuna, and M. Castilla, "Hierarchical control of droop-controlled AC and DC microgrids-a general approach toward standardization," *IEEE Trans. Ind. Electron.*, vol. 58, no. 1, pp. 158-172, Jan. 2011.

[4] Q. C. Zhong, "Robust droop controller for accurate proportional load sharing among inverters operated in parallel," *IEEE Trans. Ind. Electron.*, vol. 60, no. 4, pp. 1281-1290, Apr. 2013.

[5] J. Schiffer, R. Ortega, A. Astolfi, J. Raisch, and T. Sezi, "Conditions for stability of droop-controlled inverter-based microgrids," *Automatica*, vol. 50, no. 10, pp. 2457-2469, Orc. 2014.

[6] M. Savaghebi, A. Jalilian, J. C. Vasquez, and J. M. Guerrero, "Secondary control for voltage quality enhancement in microgrids," *IEEE Trans. Smart Grid*, vol. 3, no. 4, pp. 1893-1902, Dec. 2012.

[7] A. Bidram, A. Davoudi, F. L. Lewis, and J. M. Guerrero, "Distributed cooperative secondary control of microgrids using feedback linearization," *IEEE Trans. Power Syst.*, vol. 28, no. 3, pp. 3462-3470, Aug. 2013.

[8] S. Wen, X. Yu, Z. Zeng, and J. Wang, "Event-triggering load frequency control for multi-area power systems with communication delays," *IEEE Trans. Ind. Electron.*, vol. 63, no. 2, pp. 1308-1317, Feb. 2016.

[9] K. D. Brabandere, B. Bolsens, J. V. den Keybus, A. Woyte, J. Driesen, and R. Belmans, "A voltage and frequency droop contorl method for parallel inverters," *IEEE Trans. Power Electron.*, vol. 22, no. 4, pp. 1107-1115, Jul. 2007.

[10] C. Lee, C. Chu, and P. Cheng, "A new droop control method for the autonomous operation of distributed energy resource interface converters," *IEEE Trans. Power Electron.*, vol.28, no. 4, pp. 1980-1993, Apr. 2013.

[11] P. Vovos, A. Kiprakis, A. Wallace, and G. Harrison, "Centralized and distributed voltage control: impact on distributed generation penetration," *IEEE Trans. Power Syst.*, vol. 22, no. 1, pp. 476-483, Feb. 2007.

[12] K. Tan, X. Peng, P. So, Y. Chu, and M. Chen, "Centralized control for parallel operation of distributed generation inverters in microgrids," *IEEE Trans. Smart Grid*, vol. 3, no. 4, pp. 1977-1987, Dec. 2012.

[13] A. Vaccaro, G. Velotto, and A. F. Zobaa, "A decentralized and cooperative architecture for optimal voltage regulation in smart grids", *IEEE Trans. Ind. Electron.*, vol.58, no.10, pp. 4593-4602, Oct. 2011.

[14] H. Liang, B. J. Choi, W. Zhuang, and X. Shen, "Stability enhancement of decentralized inverter control through wireless communications in microgrids," *IEEE Trans. Smart Grid*, vol. 4, no. 1, pp. 321-331, Mar. 2013.

[15] W. Liu, W. Gu, W. X. Sheng, X. L. Meng, and Z. J. Wu, "Decentralized multi-agent system-based cooperative frequency control for autonomous microgrids with communication constraints," *IEEE Trans. Sustain. Energy*, vol.5, no.2, pp. 446-456, Apr. 2014.

[16] Q. Li, F. X. Chen, M. Y. Chen, and J. M. Guerrero, "Agent-based decentralized control method for islanded microgrids," *IEEE Trans. Smart Grid*, vol.7, no.2, pp. 637-649, Mar. 2016.

[17] C. H. Zhao, U. Topcu, N. Li, and S. Low, "Design and stability of load-side primary frequency control in power systems," *IEEE Trans. Autom. Control*, vol. 59, no. 5, pp. 1177-1189, May. 2014.

[18] V. Nasirian, Q. Shafiee, J. M. Guerrero, F. L. Lewis, and A. Davoudi, "Droop-free distributed control for AC microgrids," *IEEE Trans. Power Electronics*, vol. 31, no. 2, pp. 1600-1617, Feb. 2016.

[19] R. Olfati-Saber, and R. M. Murrary, "Consensus problem in networks of agents with switching topology and time-delays," *IEEE Trans. Autom. Control*, vol. 49, no. 9, pp. 1520-1533, Sep. 2004.

[20] X. Q. Lu, R. Q. Lu, S. H. Chen, and J. H. Lü, "Finite-time distributed tracking control for multi-agent systems with a virtual leader," *IEEE Trans. Circuits Syst. I, Reg.Papers*, vol. 60, no. 2, pp. 352-362, Feb. 2013.

[21] Q. Shafiee, J. M. Guerrero, and J. C. Vasquez, "Distributed secondary control for islanded microgrids-A novel approach," *IEEE Trans. Power Electron.*, vol. 29, no. 2, pp. 1018-1031, Feb. 2014.

[22] A. Bidram, A. Davoudi, and F. L. Lewis, "Finite-time frequency synchronization in microgrids," *IEEE Energy Conversion Congress and Exposition (ECCE)*, 2014, pp. 2648-2654.

[23] S. T. Cady, A. D. Dominguez-Garcia, and C. N. Hadjicostis, "Finite-time approximate consensus and its application to distributed frequency regulation in islanded AC microgrids," *The 48th International Conference on System Science*, pp. 2664-2670, 2015.

[24] F. H. Guo, C. Y. Wen, J. F. Mao, and Y. D. Song, "Distributed secondary voltage and frequency restoration control of droop-controlled inverter-based microgrids," *IEEE Trans. Ind. Electron.*, vol. 62, no. 7, pp. 4355-4364, Jul. 2015.

[25] W. Yao, M. Chen, J. Matas, J. Guerrero, and Z. M. Qian, "Design and analysis of the droop control method for parallel inverters considering the impact of the complex impedance on the power sharing," *IEEE Trans. Ind. Electron.*, vol. 58, no. 2, pp. 576-588, Feb. 2011.

[26] J. W. He, and Y. W. Li, "An enhanced microgrid load demand sharing strategy," *IEEE Trans. Power Electronics*, vol.27, no.9, pp. 3984-3995, Sep. 2012.

[27] Y. X. Zhu, F. Zhuo, F. Wang, B. Q. Liu, R. F. Gou, and Y. J. Zhao, "A virtual impedance optimization method for reactive power sharing in networked microgrid," *IEEE Trans. Power Electronics*, vol.31, no.4, pp. 2890-2904, Apr. 2016.

[28] H. Mahmood, D. Michaelson, and J. Jiang, "Accurate reactive power sharing in an islanded microgrid using adaptive virtual impedances," *IEEE Trans. Power Electronics*, vol.30, no.3, pp. 1605-1617, Mar. 2015.

[29] J. W. He, Y. W. Li, and F. Blaabjerg, "An enhanced islanding microgrid reactive power, imbalance power, and harmonic power sharing scheme," *IEEE Trans. Power Electronics*, vol.30, no.6, pp. 3389-3401, Jun. 2015.

[30] H. Chiang, C. Chu, and G. Cauley, "Direct stability analysis of electric power systems using energy functions: theory, applications, and perspective," *Proc. of the IEEE*, vol. 83, no. 11, pp. 1497-1529, Nov. 1995.

[31] Y. H. Moon, B. H. Cho, T. H. Rho, and B. K. Choi, "The development of equivalent system technique for deriving an energy function reflecting transfer conductances," *IEEE Trans. Power Systems*, vol. 14, no. 4, pp. 1335-1341, Nov. 1999.

[32] J. M. Guerrero, J. C. Vasquez, J. Matas, M. Castilla, and L.G. Vicuña, "Control strategy for flexible microgrid based on parallel line-interactive UPS systems," *IEEE Trans. Ind. Electron.*, vol. 56, no. 3, pp. 726-736, Mar. 2009.

[33] X. Q. Lu, Y. N. Wang, X. H. Yu, and J. G. Lai, " Finite-time control for robust tracking consensus in MASs with an uncertain leader," *IEEE Trans. Cybernetics*, 10.1109/TCYB.2016.2541693.

[34] F. Xiao, L. Wang, J. Chen, and Y. P. Gao, " Finite-time formation control for multi-agent systems," *Automatica*, vol. 45, no. 7, pp. 2605-2611, Aug. 2009.

[35] J. W. Simpson-Porco, Q. Shafiee, F. Dörfler, J. C. Vasquez, J. M. Guerrero, and F. Bullo, "Secondary frequency and voltage control of islanded microgrids via distributed averaging," *IEEE Trans. Ind. Electron.*, vol.62, no.11, pp. 7025-7038, Nov. 2015.

[36] H. Khalil, "Nonlinear systems," Prentice Hall, 2002.

[37] X. Q. Lu, F. Austin, and S. H. Chen, "Flocking in multi-agent systems with active virtual leader and time-varying delays coupling," *Commun. Nonlinear, Sci. Numer. Simulat.*, vol. 16, no. 2, pp. 1014-1026, Feb. 2011.

[38] L. Meng, T. Dragicevic, J. Roldn-Perez, J. C. Vasquez, and J. M. Guerrero, "Modeling and sensitivity study of consensus algorithm-based distributed hierarchical control for DC microgrids," *IEEE Trans. Smart Grid*, vol. 7, no. 3, pp. 1504-1515, May 2016.

[39] J. G. Lai, H. Zhou, X. Q. Lu, X. H. Yu, and W. S. Hu, "Droop-based distributed cooperative control for microgrids with time-varying delays," *IEEE Trans. Smart Grid*, vol.7, no.4, pp. 1775-1789, Jul. 2016.

[40] X. Q. Lu, X. H. Yu, J. G. Lai, J. M. Guerrero, and H. Zhou, "Distributed secondary voltage and frequency control for islanded microgrids with uncertain communication links," *IEEE Trans. Ind. Informat.*, to be published, doi: 10.1109/TII.2016.2603844, 2016.

Xiaoqing Lu received the M.Sc. and Ph.D. degrees in applied mathematics from Wuhan University, Wuhan, China.

She is currently an Associate Professor in the College of Electrical and Information Engineering, Hunan University, Changsha, China. She is also an International Exchange Research Fellow at the School of Electrical and Computer Engineering, RMIT University, Melbourne, Australia. Her research interests include nonlinear dynamical systems, intelligent systems and applications, complex networks, multi-agent systems, and microgrids.

Xinghuo Yu (M'92-SM'98-F'08) received the B.Eng. and M.Eng. degrees from the University of Science and Technology of China, Hefei, China, in 1982 and 1984, respectively, and the Ph.D. degree from Southeast University, Nanjing, China, in 1988.

He is currently with RMIT University (Royal Melbourne Institute of Technology), Melbourne, VIC, Australia, where he is Associate Deputy Vice-Chancellor Research Capability and Distinguished Professor. His current research interests include variable structure and nonlinear control, and complex and intelligent systems and applications.

Prof. Yu was a recipient of a number of awards and honors for his contributions, including the 2013 Dr.-Ing. Eugene Mittlemann Achievement Award of the IEEE Industrial Electronics Society and the 2012 *IEEE Industrial Electronics Magazine* Best Paper Award. He is President-Elect (2016-2017) of the IEEE Industrial Electronics Society.

Jingang Lai received the M.Sc. degree in control science and engineering from the Wuhan University of Technology, Wuhan, China, in 2013, and Ph.D. degree from Department of Automation, Wuhan University, Wuhan, China, in 2016. He was a Visiting Ph.D. Student in the School of Electrical and Computer Engineering, RMIT University, Melbourne, VIC, Australia, in 2015.

He is currently a Post-Doctoral Research Fellow in the School of Electrical and Electronic Engineering, Huazhong University of Science and Technology, Wuhan, China, and is also a Visiting Research Fellow in the School of Engineering, RMIT University, Melbourne, VIC, Australia. His current research interests include smart grid and networked control systems.
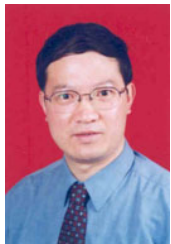
Yaonan Wang (SM'94) received the B.S. degree in computer engineering from East China Science and Technology University (ECSTU), Fuzhou, China, in 1981, and the M.S. and Ph.D. degrees in electrical engineering from Hunan University, Changsha, China, in 1990 and 1994, respectively.

He is currently a Professor with the College of Electrical and Information Engineering, Hunan University. From 1994 to 1995, he was a Post-Doctoral Research Fellow with the National University of Defense Technology, Changsha. From 1981 to 1994, he was with ECSTU. From 1998 to 2000, he was a Senior Humboldt Fellow in Germany, and from 2001 to 2004, he was a Visiting Professor with the University of Bremen, Bremen, Germany. His current research interests include intelligent control, image processing, and intelligent robotics.

Josep M. Guerrero (S'01-M'04-SM'08-F'15) received the B.S. degree in telecommunications engineering, the M.S. degree in electronics engineering, and the Ph.D. degree in power electronics from the Technical University of Catalonia, Barcelona, Spain, in 1997, 2000, and 2003, respectively.

Since 2011, he has been a Full Professor with the Department of Energy Technology, Aalborg University, Aalborg, Denmark, where he is responsible for the Microgrid Research Program. From 2012, he is a Guest Professor at the Chinese Academy of Science, Beijing, China and the Nanjing University of Aeronautics and Astronautics, Nanjing, China; from 2014, he is Chair Professor in Shandong University, Jinan, China; and from 2015, he is a Distinguished Guest Professor in Hunan University, Changsha, China. His research interests include different microgrid aspects, including power electronics, distributed energy-storage systems, hierarchical and cooperative control, energy management systems, and optimization of microgrids and islanded minigrids.

www.microgrids.et.aau.dk